# Overview of Fundamental Frequency Sensorless Algorithms for AC Motors: a Unified Perspective

Jiahao Chen, *Member, IEEE,* Xin Yuan, *Member, IEEE,* Frede Blaabjerg, *Fellow, IEEE,*
Christopher H. T. Lee, *Senior Member, IEEE*

***Abstract*—This paper uses active flux concept to review fundamental frequency sensorless algorithms for both induction and permanent magnet motors in one framework. Fundamentally, sensorless torque estimation can be *directly* solved using voltage model (VM) estimator, or *indirectly* solved using current model (CM) estimator. The latter turns the torque estimation problem into a speed estimation problem. The stator flux in VM and the $d$-axis angle in CM are deemed as the two sets of original states for sensorless drive. Through change of states, the *direct* torque estimation can be realized via observer designs; whereas the speed dependency of the unknown state (e.g., active flux and emf) gives rise to a class of speed estimation methods, known as model reference adaptive system (MRAS). The idea of a general speed observer is proposed to summarize various *separate* speed estimation methods needed for *direct* torque estimation. It is suggested to adopt inherently sensorless designs such that two-way coupling between torque estimation and speed estimation is avoided. For induction motors, it turns out the unmodelled voltage in the active flux dynamics reveals current flowing in rotor bars and can be further modelled, for which the solutions to regeneration instability problem are discussed, and change of states is recommended to attain global stability. Finally discussed are the results of slow reversal test, where local weak observability of ac motors can be potentially preserved.**

## NOMENCLATURE

The nomenclature we use is common for permanent magnet (PM) motors, where $L_d, L_q, R, \psi_{\rm PM}, \psi_{\rm A}$ are respectively $d$-axis inductance, $q$-axis inductance, stator resistance, PM flux linkage, and active flux linkage. For induction motors, $\psi_{\rm PM} = 0$, and $L_d, L_q, \psi_{\rm A}$ are redefined as stator inductance, stator transient leakage inductance, and inverse-$\Gamma$ circuit rotor flux. All **bold** $\mathbb{R}^2$ vectors are in the stator stationary $\alpha\beta$-frame, e.g., $\boldsymbol{i} = [i_\alpha, i_\beta]^\mathsf{T}$ is the measured current transformed from amplitude-invariant Clarke transformation. Park transformation is $\boldsymbol{P}(\theta_d) = \left[\begin{smallmatrix} \cos\theta_d & \sin\theta_d \\ -\sin\theta_d & \cos\theta_d \end{smallmatrix}\right]$ with $\theta_d$ as the $d$-axis angle. $\boldsymbol{J} = \left[\begin{smallmatrix} 0 & -1 \\ 1 & 0 \end{smallmatrix}\right]$, $\boldsymbol{I} = \left[\begin{smallmatrix} 1 & 0 \\ 0 & 1 \end{smallmatrix}\right]$.

## I. INTRODUCTION

Sensorless or self-sensing control is typically referring to the speed regulation of inverter-fed ac motors without using a mechanical sensor for speed (i.e., tachogenerator) or position (e.g., encoder, resolver, and hall sensor), which is especially desired for high speed motors (see e.g., [1]), motors with large-diameter or hollow shaft, and motors used in adverse environment [2].

Recently, there have been several excellent reviews [3]–[5] on sensorless control of PM motors with differentiated focuses on the applications [3], the saliency based invasive methods [4], and the non-ideal conditions [5]. Among these works, the fundamental frequency sensorless algorithms are covered with limited details. In our opinion, the nuanced differences and numerous variants of those algorithms can be understood fairly easily if one pays attention to the choice of state variables as well as the considerations behind the choice.

This paper reviews all fundamental frequency models that can be adopted for designing sensorless algorithms, and provides a solid foundation to understand all design variants for both PM motors and induction motors, with the aid of the active flux concept [6]. As a matter of fact, in induction motor context, the active flux is no new concept, and is the natural choice of state (i.e., rotor flux) with the inverse-$\Gamma$ equivalent circuit [7], and it has long been found useful in analysis, e.g., of direct torque control (DTC) [8, Eq. (7)]. In salient PM motor context, active flux has other names in literature, such as fictitious PM flux [9], linear flux [10], and extended flux [11]. The key feature that makes active flux so important is the fact that it allows to model ac motor with only one inductance, $L_q$, that dominates how fast current can change.

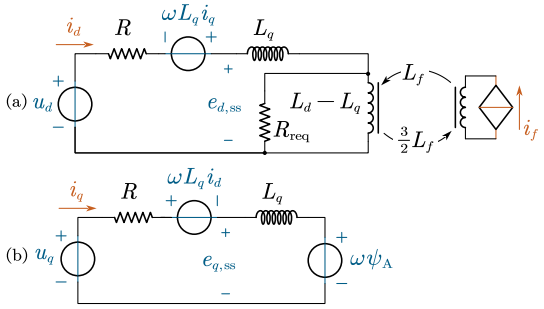


Fig. 1. The (a) $d$-axis and (b) $q$-axis equivalent circuit of the $dq$ active flux model (6). Note that the $d$-axis coil is linked with the PM linkage by $L_f i_f = \psi_{\rm PM}$.

### A. Problem Formulation

Motor's electrical angular rotor speed $\omega_r$ is governed by Newton's second law of motion:

$$J_s n_{\rm pp}^{-1} s\omega_r = T_{\rm em} - T_L \tag{1}$$

where $s = \frac{\rm d}{{\rm d}t}$ is time derivative operator, $J_s$ denotes rotor shaft inertia, $n_{\rm pp}$ designates pole pair number, $T_L$ is load torque, and $T_{\rm em}$ is electromagnetic torque. The torque by DTC is proportional to cross product of the stator flux $\boldsymbol{\psi}_s$ and the active flux $\boldsymbol{\psi}_{\rm A}$:

$$T_{\rm em} = \underbrace{\tfrac{3}{2} n_{\rm pp} L_q^{-1} \boldsymbol{\psi}_s \cdot (-\boldsymbol{J}\boldsymbol{\psi}_{\rm A})}_{\text{DTC formulation}} = \underbrace{\tfrac{3}{2} n_{\rm pp} \psi_{\rm A} i_q}_{\text{FOC formulation}} \tag{2}$$

with $i_q = -i_\alpha \sin\theta_d + i_\beta \cos\theta_d$ as the $q$-axis current, where the field oriented control (FOC) formulation is derived by substituting the following relation between $\boldsymbol{\psi}_s$ and $\boldsymbol{\psi}_{\rm A}$ [6]

$$\boldsymbol{\psi}_s - L_q \boldsymbol{i} = \boldsymbol{\psi}_{\rm A} \triangleq \psi_{\rm A} \begin{bmatrix} \cos\theta_d \\ \sin\theta_d \end{bmatrix} \tag{3}$$

Here, the polar coordinate definition of active flux $\boldsymbol{\psi}_{\rm A}$ assumes fundamental frequency model, and the angle of active flux vector $\boldsymbol{\psi}_{\rm A}$ is used as the $d$-axis angle for field orientation in FOC.

Sensorless control of system (1) is challenging, because neither the input $T_{\rm em}$ nor the output $\omega_r$ is known. The objective of a sensorless algorithm is to estimate $T_{\rm em}$ and $\omega_r$. Motion equation (1) cannot be used for torque estimation because there exists an unknown term $T_L$, and therefore we shall seek for other models.

### B. Choice of Original States

Now we are faced with the first choice of state variables. If we accept FOC formulation, making $\psi_{\rm A}$ and $\theta_d$ the states, active flux

in (3) can be described by the current-speed model (CM):

$$\psi_{\rm A} = \frac{1}{\frac{(L_d-L_q)}{R_{\rm req}}s+1}\left(L_d - L_q\right) i_d + \psi_{\rm PM} \tag{4a}$$

$$\theta_d = \frac{1}{s}\omega = \int \left(\omega_r + \omega_{\rm sl}\right) {\rm d}t \tag{4b}$$

with $i_d = i_\alpha \cos\theta_d + i_\beta \sin\theta_d$ as the $d$-axis current, $R_{\rm req}$ the inverse-$\Gamma$ circuit rotor resistance, $\omega \triangleq s\theta_d$ the synchronous speed, and $\omega_{\rm sl}$ the slip speed. For induction motors, there is a low pass filter (LPF) with a time constant of $\frac{L_d-L_q}{R_{\rm req}}$ applied to the coil excitation in (4a), and only in this case the slip relation $\omega_{\rm sl} = \frac{R_{\rm req} i_q}{\psi_{\rm A}}$ is valid. For inverter-fed PM motors, it is valid to simply put $R_{\rm req} = \infty$, $\omega_{\rm sl} = 0$, and $\omega = \omega_r$.

If the DTC formulation is adopted, making $\boldsymbol{\psi}_s$ the state, as per Faraday's law, the stator voltage equation in $\alpha\beta$-frame serves as the voltage-current model (VM) of active flux:

$$\boldsymbol{\psi}_{\rm A} + L_q \boldsymbol{i} \overset{(3)}{=} \boldsymbol{\psi}_s = \tfrac{1}{s}\boldsymbol{e}_s = \tfrac{1}{s}(\boldsymbol{u} - R\boldsymbol{i}) \tag{5}$$

where $\boldsymbol{e}_s \triangleq s\boldsymbol{\psi}_s$ is stator emf, and $\boldsymbol{u}$ is $\alpha\beta$-frame stator voltage.

Therefore, the torque estimation problem is solved by either:

- estimating $d$-axis position $\theta_d$ and $\psi_{\rm A}$ using CM (4), or
- estimating stator flux $\boldsymbol{\psi}_s$ (and $\boldsymbol{\psi}_{\rm A}$) using VM (5).

Determining $d$-axis angle in a feed-forward fashion as (4b) is called indirect field orientation (IFO). The IFO solves the torque estimation *indirectly* via speed estimation. Counter-intuitively, the VM in $dq$-frame can be used to estimate field speed $\omega$. To see this, applying Park transformation $\boldsymbol{P}(\theta_d)$ to VM (5) yields:

$$s\psi_{\rm A} + L_q s i_d = u_d - R i_d + \omega L_q i_q \triangleq e_{d,\rm ss} \tag{6a}$$

$$\omega\psi_{\rm A} + L_q s i_q = u_q - R i_q - \omega L_q i_d \triangleq e_{q,\rm ss} \tag{6b}$$

where $e_{d,\rm ss}, e_{q,\rm ss}$ are steady-state auxiliary emfs in $dq$-frame, and can be used for estimating $\omega$. Fig. 1 shows the equivalent circuit of the $dq$ model (6), where (4a) has been elaborated as a mutual linkage and a parallel RL circuit in Fig. 1a. Fig. 1b shows the active power passing through motor air gap is $\frac{3}{2}\omega\psi_{\rm A} i_q$, [cf. (2)].

On the other hand, implementing $\theta_d = \arctan2(\psi_{\beta\rm A}, \psi_{\alpha\rm A})$ is called direct field orientation (DFO). The IFO and DFO use the same information, i.e., measured voltage and current, but in different manners. The key difference is that the DFO can be made explicitly independent of motor speed and speed error, because there is no speed variable in (5), which facilitates speed-independent *direct* torque estimation.

### C. Change of States

Alternatively, we may select current $\boldsymbol{i}$ and active flux $\boldsymbol{\psi}_{\rm A}$ as the new states for torque estimation. Taking time derivative of (3) derives the active flux dynamics in (7a), and substituting (3) into the VM (5) gives the output dynamics in (7b).

$$s\boldsymbol{\psi}_{\rm A} = \omega\boldsymbol{J}\boldsymbol{\psi}_{\rm A} + \underbrace{(s\psi_{\rm A})\begin{bmatrix}\cos\theta_d \\ \sin\theta_d\end{bmatrix}}_{\boldsymbol{E}_u} \tag{7a}$$

$$L_q s\boldsymbol{i} = \boldsymbol{e}_s - s\boldsymbol{\psi}_{\rm A} = \boldsymbol{e}_s - \omega\boldsymbol{J}\boldsymbol{\psi}_{\rm A} - \boldsymbol{E}_u \tag{7b}$$

where $\boldsymbol{E}_u$ denotes the unmodelled dynamics. From (7), ac motor appears to be modelled with one inductance, $L_q$. As we will see later, $\boldsymbol{\psi}_{\rm A}$ is only one example of many choices of state changes, and alternative choices include the "active emf" $\boldsymbol{e}_{\rm A} \triangleq s\boldsymbol{\psi}_{\rm A}$ or the extended emf $\boldsymbol{e}_{\rm E}$ in Appendix A. Nevertheless, the key idea here is that by explicitly selecting the system output $\boldsymbol{i}$ as state, the torque estimation problem can now be solved by designing:

- a full- or reduced-order state observer using (7); or
- a disturbance observer using only the output equation (7b).

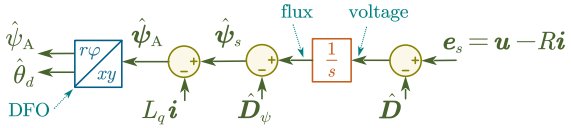


Fig. 2. Block diagram of a general stabilized VM flux estimator for DFO.

### D. Coupling with Speed Estimation

From (7), the synchronous speed $\omega \triangleq s\theta_d$ appears to be an inherent parameter of ac motors. As a result, speed estimation can be achieved by

- estimating $\omega_r$ (and $T_L$) as state using (1) and $s\theta_d = \omega$; or,
- estimating $\omega$ as a constant parameter (note $\omega_r = \omega - \omega_{\rm sl}$).

Direct torque estimation using (5) offers a possibility for being independent on its ensuing *separate* speed estimation, which is preferred as stabilities of torque estimation and speed estimation can be analyzed separately. On the other hand, the speed dependencies, e.g., in model (6) and (7a), imposes to estimate torque and speed *jointly* (using either DFO or IFO), leading to complicated stability analysis. In fact, there is a convention in most sensorless PM motor literature, that is, the stability analysis of the two-way coupling between the joint estimation of torque and speed is not performed. The first part of this paper will follow this convention to help the readers better understand the literature, while rigorous analysis of the interconnected estimators is reviewed in the second part (Section V), dedicated to sensorless induction motors. Fortunately, the induction motor oriented analysis can be potentially transferred to PM motor, as is exemplified in [12].

## II. Design in Original States

A stator flux estimate can be obtained by integrating $\boldsymbol{e}_s$, but the estimate $\frac{1}{s}\boldsymbol{e}_s$ is unbounded in practice. There are two approaches to stabilize the integration, i.e., the time-domain approach and the frequency-domain approach, where several steady state assumptions are often resorted to, including:

(i) constant $\psi_{\rm A}$ assumption, thus the active flux trajectory (i.e., its Lissajous curve) is circular about origin;
(ii) orthogonality between flux and emf: $\boldsymbol{e}_{\rm A} = \omega\boldsymbol{J}\boldsymbol{\psi}_{\rm A}$; and
(iii) orthogonality between $\alpha\beta$-axes emfs: $s\boldsymbol{e}_{\rm A} = \omega\boldsymbol{J}\boldsymbol{e}_{\rm A}$.

### A. VM Estimator in Time-Domain

Let $\hat{}$ denote estimated value. As shown in Fig. 2, the integrator is stabilized at both its input and output:

$$\hat{\boldsymbol{\psi}}_s = \hat{\boldsymbol{\psi}}_{\rm A} + L_q\boldsymbol{i} = \int_0^t \left(\boldsymbol{u} - R\boldsymbol{i} - \hat{\boldsymbol{D}}\right){\rm d}t - \hat{\boldsymbol{D}}_\psi \tag{8}$$

where the flux compensation $\hat{\boldsymbol{D}}_\psi$ is used to offset the center of the estimated flux trajectory, and the voltage compensation $\hat{\boldsymbol{D}}$ is added to remove the unmodelled dc drift $\boldsymbol{D}$ in $\boldsymbol{e}_s$, e.g., due to thermal drift in analog devices. When there is a drift $\boldsymbol{D}_\psi = \int_0^t \boldsymbol{D}{\rm d}t$ in the flux estimate, the resulting errors in position and speed estimation can be derived as in [13, Eqs. (19), (21)]. Typical generation processes of $\hat{\boldsymbol{D}}_\psi$ and $\hat{\boldsymbol{D}}$ are summarized in Fig. 3.

*1) Correction by Flux Trajectory Center:* A corollary of the constant flux amplitude assumption is that an accurate $\alpha$-axis flux estimate results in a sinusoidal waveform whose maximum and

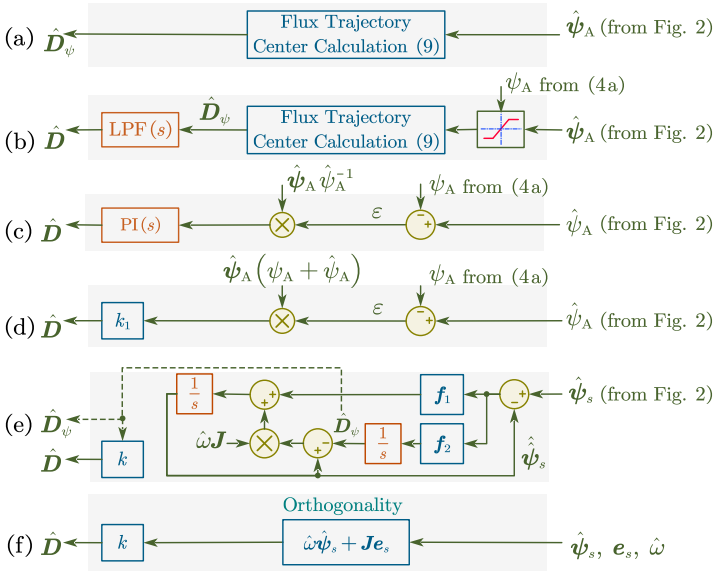


Fig. 3. Block diagrams of generation of $\hat{\boldsymbol{D}}$ and $\hat{\boldsymbol{D}}_\psi$. Flux trajectory center calculation based (a) flux and (b) voltage compensation; (c) (d) two main variants of flux amplitude mismatch $\varepsilon$ based voltage compensation; (e) state observer for $\boldsymbol{D}_\psi$ with $\boldsymbol{f}_1, \boldsymbol{f}_2$ the gain matrices; (f) orthogonality based voltage compensation.

minimum add up to null. In other words, the center of the flux estimate *over one electrical cycle*, i.e.,

$$\hat{\boldsymbol{D}}_\psi = \begin{bmatrix} \hat{D}_{\alpha\psi} \\ \hat{D}_{\beta\psi} \end{bmatrix} = \frac{1}{2} \begin{bmatrix} \max\left(\hat{\psi}_{\alpha\mathrm{A}}\right) + \min\left(\hat{\psi}_{\alpha\mathrm{A}}\right) \\ \max\left(\hat{\psi}_{\beta\mathrm{A}}\right) + \min\left(\hat{\psi}_{\beta\mathrm{A}}\right) \end{bmatrix} \tag{9}$$

should be $\mathbf{0}$. One can directly use $\hat{\boldsymbol{D}}_\psi$ in (9) to produce a final flux estimate as $\frac{1}{s}\boldsymbol{e}_s - \hat{\boldsymbol{D}}_\psi$ [13] (see Fig. 3a), or one can use it to construct a voltage compensation as $\hat{\boldsymbol{D}} = \mathrm{LPF}(s)\hat{\boldsymbol{D}}_\psi$ [14] (see Fig. 3b). In fact, the voltage compensation error $\boldsymbol{D} - \hat{\boldsymbol{D}}$ can be exactly calculated from $\hat{\boldsymbol{D}}_\psi$ by further utilizing time information, as illustrated in [15, Fig. 4]. As is discussed in [16, Sec. III], it is better to use active flux instead of stator flux to calculate $\hat{\boldsymbol{D}}_\psi$ in (9), because stator flux components are not sinusoidal when current sudden changes.

*2) Correction by Amplitude Mismatch:* Assuming $\psi_\mathrm{A}$ and $\hat{\psi}_\mathrm{A}$ are respectively available from (4a) and Fig. 2, the active flux amplitude mismatch $\varepsilon = \hat{\psi}_\mathrm{A} - \psi_\mathrm{A}$ can be used to generate a voltage compensation, as shown in Fig. 3c [6], [17]–[30]:[1]

$$\hat{\boldsymbol{D}} = \mathrm{PI}\,(s)\,\frac{\hat{\boldsymbol{\psi}}_\mathrm{A}}{\hat{\psi}_\mathrm{A}}\varepsilon, \text{ with } \mathrm{PI}\,(s) \triangleq k_1 + \frac{k_2}{s},\ k_1, k_2 > 0 \tag{11}$$

Note for induction motors, the calculated $\psi_\mathrm{A}$ is often rendered as the flux command [31], [32]. VM estimator (8) plus correction (11) describes the so-called *hybrid flux estimator* that outputs the sum of high-pass filtered VM estimate and low-pass filtered "CM" estimate, and leads to the classical interpretation that VM is used for high speeds and "CM" is used for low speeds [18]–[21], [23]. It is worth pointing out there exists an abuse use of the term "CM". In PM motor literatures, the "CM" estimate is often written in $dq$-frame and does not provide any angle information (see e.g., [23, Eq. (10)]), which is distinct from the CM (4) expressed in polar-

[1]The flux amplitude mismatch $\varepsilon = \hat{\psi}_\mathrm{A} - \psi_\mathrm{A}$ from (11) has an equivalent current error form as shown in (10b), if a current estimate $\hat{\boldsymbol{i}}$ is introduced as (10a):

$$\hat{\boldsymbol{i}} = L_q^{-1}\left(\hat{\boldsymbol{\psi}}_s - \frac{\hat{\boldsymbol{\psi}}_\mathrm{A}}{\hat{\psi}_\mathrm{A}}\psi_\mathrm{A}\right), \text{ note: } \frac{\hat{\boldsymbol{\psi}}_\mathrm{A}}{\hat{\psi}_\mathrm{A}} = \begin{bmatrix} \cos\hat{\theta}_d \\ \sin\hat{\theta}_d \end{bmatrix} \tag{10a}$$

$$\boldsymbol{i} - \hat{\boldsymbol{i}} = L_q^{-1}\hat{\boldsymbol{\psi}}_\mathrm{A}\left(\frac{\psi_\mathrm{A}}{\hat{\psi}_\mathrm{A}} - 1\right) = -L_q^{-1}\frac{\hat{\boldsymbol{\psi}}_\mathrm{A}}{\hat{\psi}_\mathrm{A}}\varepsilon \tag{10b}$$

which is used, e.g., in [25] to build a sliding mode variant of (11).

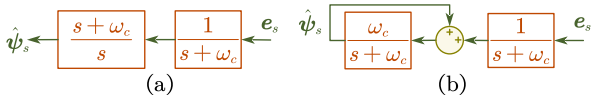


Fig. 4. (a) Multiplicative and (b) additive equivalent form of an integrator $\frac{1}{s}$. Note $\hat{\boldsymbol{\psi}}_s$ is unbounded in practice for both cases.

coordinates. Discussions for selection of $k_1, k_2$ are documented in [17]–[19], and it is suggested in [17], [18], [31] to set $k_2$ to zero. Coincidentally, a contribution from the control community also suggests to not implement the $k_2$ integral term, but in a slightly different form from (11) as shown in Fig. 3d, to facilitate the stability analysis [33], [34]:

$$\hat{\boldsymbol{D}} = k_1\hat{\boldsymbol{\psi}}_\mathrm{A}\left(\hat{\psi}_\mathrm{A} + \psi_\mathrm{A}\right)\varepsilon = k_1\hat{\boldsymbol{\psi}}_\mathrm{A}\left(\hat{\psi}_\mathrm{A}^2 - \psi_\mathrm{A}^2\right) \tag{12}$$

However, note the $k_2 = 0$ design results in a non-zero bias in flux estimate in practice. The integrator $\frac{k_2}{s}$ or another dedicated "offset extractor" [32] can be used to eliminate the flux bias.

The VM estimator (8) corrected by (11) or (12) is speed-independent, but it is possible to introduce speed-dependency by transforming (8) into $dq$-frame. In [35], [36], the current error in (10) is used to build a speed-adaptive VM estimator in $dq$-frame.

*3) State Observer for Flux Offset $\boldsymbol{D}_\psi$:* Assume there is an offset $\boldsymbol{D}_\psi$ existing in the biased VM flux estimate $\hat{\boldsymbol{\psi}}_s$, which satisfies following steady state speed-dependent dynamics [37]:

$$s\hat{\boldsymbol{\psi}}_s = \hat{\omega}\boldsymbol{J}\left(\hat{\boldsymbol{\psi}}_s - \boldsymbol{D}_\psi\right), \quad s\boldsymbol{D}_\psi = \boldsymbol{D} \approx 0 \tag{13}$$

where it is assumed that $\boldsymbol{D}_\psi$ is slowly varying and that the orthogonality between the $\alpha$- and $\beta$-axes of the flux holds. Fig. 3e shows a state observer using (13), which is also known as the *frequency-adaptive observer* in literature [23]. The observer tuning (or pole placement) in [37] is dependent on $\hat{\omega}$, thus sensitivity with respect to speed error has been analyzed. One can understand the VM along with its frequency-adaptive observer as a "single tune integrator" with a mandatory dependency on $\hat{\omega}$ [38], [39]. Readers are referred to [5, Table 4] for a review of frequency-adaptive observers for eliminating emf harmonics.

*4) Correction by Orthogonality:* The speed-dependent vector orthogonality condition $\hat{\omega}\hat{\boldsymbol{\psi}}_s + \boldsymbol{J}\boldsymbol{e}_s = \mathbf{0}$ can be used to generate voltage compensation $\hat{\boldsymbol{D}}$ [40], [41], as shown in Fig. 3f.

### B. VM Estimator in Frequency-Domain

In order to stabilize the pure integration, a high pass filter (HPF) can be added to the output of the VM estimator [42], which is equivalent to replacing the integrator with an LPF:

$$\hat{\boldsymbol{\psi}}_s = \underbrace{\frac{\omega_c s}{s+\omega_c}}_{\mathrm{HPF}} \times \frac{1}{s}\boldsymbol{e}_s = \underbrace{\frac{\omega_c}{s+\omega_c}}_{\mathrm{LPF}}\boldsymbol{e}_s \tag{14}$$

which is speed-independent if a fixed cut-off frequency $\omega_c$ is used. In fact, it is reported that placing the LPF pole $-\omega_c$ to be close to zero is sufficient for zero speed operation of induction motor [43], but it is also recommended to adopt the speed-dependent tuning $\omega_c = k|\hat{\omega}|,\ k > 0$ to adjust observer damping with respect to operating speed [44], [45].

The LPF in (14) is stable but introduces undesired lag and gain. The two equivalent forms of an integrator, as shown in Fig. 4, serve as a starting point to design two types of frequency-domain compensations for (14).

*1) Multiplicative Compensation:* Let $j = \sqrt{-1}$. Allow an abuse of notation between complex number and $\mathbb{R}^2$ vector, i.e., $\boldsymbol{e}_s =$

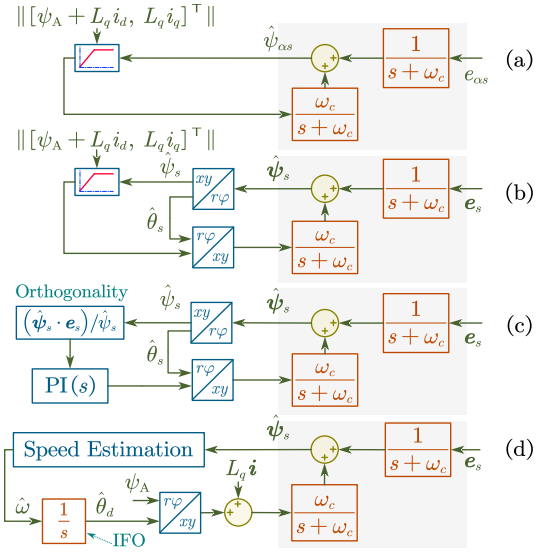


Fig. 5. Additive compensations variants. (a) Component-wise limiter; (b) amplitude limiter; (c) orthogonality based, and (d) CM estimator based correction.

$[e_{\alpha s}, e_{\beta s}]^{\mathsf{T}} = e_{\alpha s} + je_{\beta s}$. Then, the multiplicative compensation can be introduced at steady state as follows (cf. Fig. 4a) [44]–[49]:

$$\hat{\boldsymbol{\psi}}_s = \frac{j\hat{\omega} + k\,|\hat{\omega}|}{j\hat{\omega}} \frac{1}{s + k\,|\hat{\omega}|} (e_{\alpha s} + je_{\beta s}) = \frac{[\boldsymbol{I} - k\boldsymbol{J}\,\mathrm{sign}\,(\hat{\omega})]\,\boldsymbol{e}_s}{s + k\,|\hat{\omega}|} \quad (15)$$

which is speed-dependent and can be regarded as a single-tune integrator in a sense that its frequency response at $\hat{\omega}$ is the same as $\frac{1}{s}$. Estimator (15) is also called *statically compensated VM* [45], [50] as the compensation is only exact at steady state. It is suggested in [47] to apply the static compensation to the stator emf $\boldsymbol{e}_s$ first before going through the LPF. Advice for selecting $k$ in (15) is given in [45], [47], [48]. In [51], three speed-dependent cascaded LPFs are used to recover the desired frequency response of a pure integrator.

The presence of skew-symmetric matrix $\boldsymbol{J}$ in (15) means that, e.g., $\beta$-axis emf is used for compensating $\alpha$-axis dynamics and vice versa, which implies the orthogonality has been assumed. However, if some signal phase shift network is introduced, the compensation can be accomplished within the same axis, and therefore even elliptical flux trajectory can be tracked [52].

*2) Additive Compensation:* In Fig. 4b, the output signal $\hat{\boldsymbol{\psi}}_s$ is unbounded, and an idea to stabilize the system is to use a bounded signal in replace of $\hat{\boldsymbol{\psi}}_s$ that is being fed-back to $\frac{\omega_c}{s+\omega_c}$. Typical ideas to generate a stable flux signal have been presented in Fig. 5. The component-wise limiter in Fig. 5a distorts the flux waveform, while the amplitude limiter in Fig. 5b does not correct flux angle [53]. Fig. 5c exploits the orthogonality between flux and emf to estimate the flux amplitude [53], for which deteriorated performance in transients has been reported [17]. Fig. 5d shows a VM estimator utilizing the CM estimator output as the stable signal [31]. Fig. 5d is an example of using both the amplitude and angle information of the CM (4) (in polar coordinate) for correcting VM estimator, while the compensation (11) only utilizes the amplitude information of the CM, as an effort to avoid speed dependency.

### C. CM Estimator

Theoretically, the CM (4) can calculate flux amplitude and angle without any voltage information, but it is practically impossible to be implemented without access to the VM equation. Typically, CM is implemented by estimating speed in the IFO $dq$-frame, i.e., the $d$-axis angle of the reference frame is determined as the integral of a speed estimate: $\hat{\theta}_d = \frac{1}{s}\hat{\omega}$.

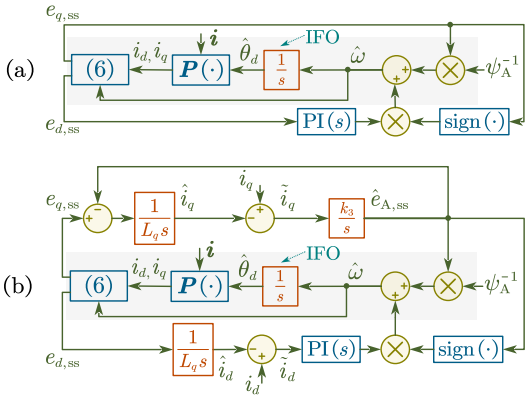


Fig. 6. CM estimator implemented with (a) direct calculation of speed, and (b) the $dq$-frame current prediction (i.e., open loop observer).

*1) CM with Constant dq-Frame Current:* Assume $si_d = si_q = s\psi_{\mathrm{A}} = 0$, and the field speed can then be directly calculated at the current step according to (6):

$$\hat{\omega} = e_{q,\mathrm{ss}}/\psi_{\mathrm{A}}, \quad \text{if } e_{d,\mathrm{ss}} = 0 \quad (16)$$

If $e_{d,\mathrm{ss}} \neq 0$, then the IFO $d$-axis angle $\hat{\theta}_d = \frac{1}{s}\hat{\omega}$ must be corrected by a feedback loop to force $e_{d,\mathrm{ss}} = 0$. One practical implementation of (16) is shown in Fig. 6a [54, Sec. III] [55]:

$$s\hat{\theta}_d = \hat{\omega} = k\frac{e_{q,\mathrm{ss}}}{\psi_{\mathrm{A}}} + \mathrm{sign}(e_{q,\mathrm{ss}})\frac{k_1 s + k_2}{s} e_{d,\mathrm{ss}} \quad (17)$$

Special choices are $k = 0$ [1], [56], and $k = 1, k_2 = 0$ [50], [57]. Practical consideration during starting is provided in [56]. The fact that $e_{q,\mathrm{ss}}$ relies on $\hat{\omega}$, makes $\hat{\omega}$ appear on both side of (17), resulting in an algebraic loop, which can be resolved by introducing an additional LPF in (17) [45].

*2) CM with Dynamic dq-Frame Current:* It is possible to remove the assumption $si_d = si_q = 0$ for (17). To this end, the $d$-axis correction is driven by $d$-axis current error $\tilde{i}_d = i_d - \hat{i}_d$ [see (18a)], and $q$-axis emf $e_{q,\mathrm{ss}}$ is replaced with an active emf amplitude estimate $\hat{e}_{\mathrm{A,ss}}$ that is proportional to the integral of $q$-axis current error $\tilde{i}_q = i_q - \hat{i}_q$ [see (18b)]: [54, Sec. IV]

$$s\hat{\theta}_d = \hat{\omega} = \frac{\hat{e}_{\mathrm{A,ss}}}{\psi_{\mathrm{A}}} + \mathrm{sign}(\hat{e}_{\mathrm{A,ss}})\frac{k_1 s + k_2}{s}\left[i_d - \frac{1}{L_q s} e_{d,\mathrm{ss}}\right] \quad (18a)$$

$$\hat{e}_{\mathrm{A,ss}} = \frac{k_3}{s}\left[i_q - \frac{1}{L_q s}(e_{q,\mathrm{ss}} - \hat{e}_{\mathrm{A,ss}})\right] \quad (18b)$$

where note $k_2$ is originally set to zero in [54]. Note the one-step current predictions are embedded in (18) as $L_q s\hat{i}_q = e_{q,\mathrm{ss}} - \hat{e}_{\mathrm{A,ss}}$ and $L_q s\hat{i}_d = e_{d,\mathrm{ss}}$, as is clarified in Fig. 6b [54] [58, Sec. 9.2.2]. Speed dependent gain $k_2(\hat{\omega})$ has been suggested in [59]. In addition, closed-loop current observer can be implemented instead of the open-loop current predictions [60], [61], and moreover, in [60], the motion equation (1) is exploited to modify (18a) for better dynamic performance, if inertia $J_s$ is provided.

It is one of the most interesting observations in the field of sensorless control, that (when $\psi_{\mathrm{A}}$ is constant) the open-loop $q$-axis current prediction in (18b) contains field speed error information, and the open-loop $d$-axis current prediction in (18a) contains position error information (see [58, Eq. (9.26)] [31, Fig. 6] [56]). This can be further generalized for time-varying $\psi_{\mathrm{A}}$ scenario as "basic relations for sensorless flux estimation" [45, Eq. (13)].

*3) Other CM Estimators:* The CM estimator $\hat{\theta}_d = \frac{1}{s}\hat{\omega}$ turns torque estimation problem into a speed estimation problem given an $d$-axis angle estimate $\hat{\theta}_d$. Therefore, the $dq$ frame speed-adaptive VM estimator in [35], [36] can be used to establish a CM estimator, as is done in [62]. Technically speaking, the CM

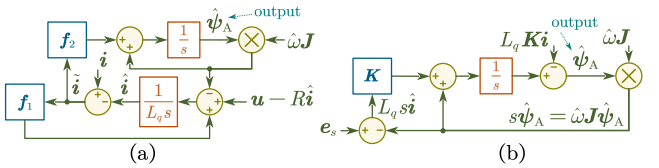


Fig. 7. (a) Full-order and (b) reduced-order state observer for active flux $\boldsymbol{\psi}_{\mathrm{A}}$.

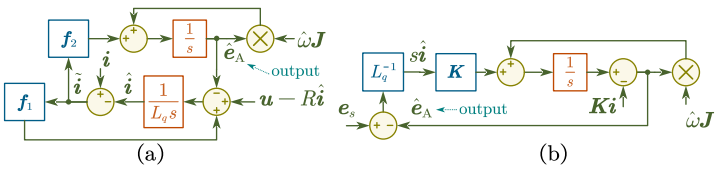


Fig. 8. (a) Full-order and (b) reduced-order state observer for active emf $\boldsymbol{e}_{\mathrm{A}}$.

inspired speed estimation prefers to be implemented in $dq$-frame. Using no correction in the CM estimator (i.e., $\hat{\theta}_d = \frac{1}{s}\hat{\omega} + 0$) is generally suggested [60], but outlier does exist, e.g., [63, Eq. (17)].

## III. Design via Change of States

The current dynamics (7b) are disturbed by an unknown emf disturbance $\boldsymbol{e}_{\mathrm{A}} \triangleq s\boldsymbol{\psi}_{\mathrm{A}}$. There are two ensuing ideas to deal with it, i.e., state observer and disturbance observer. The latter does not need a model for disturbance thus is potentially speed-independent; while the former becomes speed-dependent as it models the disturbance as either a flux or emf state.

### A. State Observer for Flux

Using (7), a flux state observer can be implemented in full-order form [9], [10], [64], [65], or reduced-order form [66]. Fig. 7a shows that full-order observer is corrected by current error $\tilde{\boldsymbol{i}} = \boldsymbol{i} - \hat{\boldsymbol{i}}$ with correction functions $\boldsymbol{f}_1, \boldsymbol{f}_2 \in \mathbb{R}^2$. Fig. 7b implies that reduced-order observer is in effect corrected by the current time-derivative error $(s\boldsymbol{i} - s\hat{\boldsymbol{i}})$ with the gain matrix $\boldsymbol{K} \in \mathbb{R}^{2\times 2}$.

*1) Full-order Flux Observer Variants:* In [9], the observer is analyzed by Lyapunov stability theory through finding the positive-definite matrix for the Kalman-Yakubovich lemma. In [65], [67], sliding mode (SM) flux state observer that has nonlinear $\boldsymbol{f}_1, \boldsymbol{f}_2$ is proposed, and the pole placement for robustness improvement is detailed in [67]. In [64], the flux state observer is implemented in $\gamma\delta$-frame, and in particular, the speed difference between $dq$-frame and $\gamma\delta$-frame that arises during speed transients is estimated by a separate speed state observer.

*2) Reduced-order Flux Observer Design:* In [66], the reduced-order flux observer is analyzed in the misaligned $\gamma\delta$-frame, and is described by a rotatory differential operator: $\boldsymbol{P}(\theta)\, s\boldsymbol{P}^{-1}(\theta) = s\boldsymbol{I} + (s\theta)\boldsymbol{J}$, where the stability analysis (that suggests $\boldsymbol{K} = k_1\boldsymbol{I} - k_2 \mathrm{sign}(\hat{\omega})\,\boldsymbol{J}$) holds only if speed is already known: $\hat{\omega} = \omega$.

### B. State Observer for EMF

Differentiating the active flux dynamics (7a) yields the active emf dynamics (19b) and its corresponding output equation (19a):

$$L_q s\boldsymbol{i} = \boldsymbol{u} - R\boldsymbol{i} - \boldsymbol{e}_{\mathrm{A}} \tag{19a}$$

$$s\boldsymbol{e}_{\mathrm{A}} = \omega\boldsymbol{J}\boldsymbol{e}_{\mathrm{A}} + \underbrace{(s\omega)\boldsymbol{J}\boldsymbol{\psi}_{\mathrm{A}} + s\boldsymbol{E}_u}_{\text{Unmodelled dynamics}} \tag{19b}$$

where the unmodelled dynamics appear during speed transients, but are often neglected in state observer design. The $d$-axis angle is recovered by integrating emf: $\int \boldsymbol{e}_{\mathrm{A}} \mathrm{d}t$, or directly calculated as

$$\theta_d = -\arctan 2\left(\frac{e_{\alpha\mathrm{A}}}{\mathrm{sign}(\omega)}, \frac{e_{\beta\mathrm{A}}}{\mathrm{sign}(\omega)}\right) \tag{20}$$

Note constant active flux amplitude (i.e., $s\psi_{\mathrm{A}} = 0$) has been implicitly assumed in (20). Note the extended emf $\boldsymbol{e}_{\mathrm{E}}$ in Appendix A can also be substituted in (20).

From the perspective of state observer design, the differences between an active emf observer and an extended emf observer are minor, so there is no need to differentiate between the two, and in fact their reduced-order state observers share the same form:

$$s\hat{\boldsymbol{e}}_{\mathrm{X}} = \hat{\omega}\boldsymbol{J}\hat{\boldsymbol{e}}_{\mathrm{X}} - \boldsymbol{K}L_q\left(s\boldsymbol{i} - s\hat{\boldsymbol{i}}\right) \tag{21}$$

where the subscript X is placeholder of the letter A or E. The implementation of active emf observers is shown in Fig. 8.

Full-order emf state observers are widely studied [68]–[74], while the reduced-order form stays as a classic [75], [76]. The key difference between full-order and reduced-order lies in how they treat speed error. Full-order observer reconstructs a current estimate $\hat{\boldsymbol{i}}$, and calculate the output error $\tilde{\boldsymbol{i}}$ that is used to tune a speed estimate $\hat{\omega}$. This requires that $\tilde{\boldsymbol{i}}$ is *sensitive to speed error*. On the other hand, since current $\boldsymbol{i}$ is measured, there is no need to reconstruct an estimate $\hat{\boldsymbol{i}}$, and the unknown state is directly estimated by (21), assuming that a speed estimate $\hat{\omega}$ is available. This needs the state estimate $\hat{\boldsymbol{e}}_{\mathrm{X}}$ to exhibit *robustness against speed error* via careful observer pole placement [76].

*1) Full-order EMF Observer Variants:* Linear corrections $\boldsymbol{f}_1, \boldsymbol{f}_2$ are beneficial for analysis and tuning [64], [68]–[70], In [68], linear system analysis is conducted to tune the observer. The $\gamma\delta$-frame implementation of the emf observer can be found in [64], where included is an interesting study that analyzes the consequences of using constant speed assumption in emf observer. In [69], the influence of dc offset on emf estimation is analyzed. In [70], observer steady-state errors are analyzed considering current/votlage error, parameter uncertainty and filtering. Nonetheless, nonlinear SM corrections are also proposed [71]–[74], among which time-varying gain is used in [73] to reduce chattering. It is worth noting that excessive correction in current estimate dynamics reduces $\tilde{\boldsymbol{i}}$'s sensitivity to speed error. In extreme case, $\tilde{\boldsymbol{i}}$ is forced to be zero (e.g., trapped in SM surface), so that there is no way to extract speed information from $\tilde{\boldsymbol{i}}$ (but is still possible to extract from the correction terms).

*2) Reduced-order EMF Observer Designs:* By assuming that $s\boldsymbol{e}_{\mathrm{A}} = \boldsymbol{0}$, Tomita *et al.* [75] proposed a reduced-order observer, for which the speed-dependent pole placement was mandatory, and was derived by analyzing the $H_\infty$ norm of transfer function from the unmodelled dynamics to the estimated emf error. Similar $H_\infty$ norm based pole placement is used in [76] to design a reduced-order observer for the extended emf model (37) to preserve its robustness against speed error.

### C. Disturbance Observer

The idea of classical disturbance observer (DO or DOB) is to simply solve for the unknown term using the output equation (7b) or (19a), and to avoid pure differentiation, an LPF is inserted:

$$\hat{\boldsymbol{e}}_{\mathrm{A}} = \mathrm{LPF}(s)\left(\boldsymbol{e}_s - L_q s\boldsymbol{i}\right) \tag{22}$$

Reduced-order state observer can be deemed as a special case of (22), if $\mathrm{LPF}(s)$ is generalized to an $\mathbb{R}^{2\times 2}$ transfer function matrix:

$$\hat{\boldsymbol{e}}_{\mathrm{A}} = \underbrace{\left[s\boldsymbol{I} - (\hat{\omega}\boldsymbol{J} - \boldsymbol{K})\right]^{-1}\boldsymbol{K}}_{\text{In replace of the LPF}(s)\text{ in (22)}}\left(\boldsymbol{e}_s - L_q s\boldsymbol{i}\right) \tag{23}$$

where the speed dependency has been introduced.

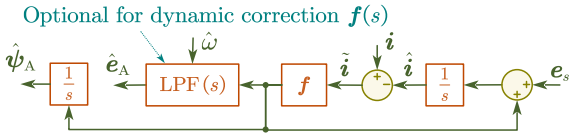


Fig. 9. Disturbance observer in output correction form for estimating active emf.

In addition to the classical form (22), DO has an alternative form being a current observer with output correction $\boldsymbol{f}(\tilde{\boldsymbol{i}})$:

$$L_q s\hat{\boldsymbol{i}} = \boldsymbol{u} - R\hat{\boldsymbol{i}} + \boldsymbol{f}(\tilde{\boldsymbol{i}}), \quad \text{with } \tilde{\boldsymbol{i}} \triangleq \boldsymbol{i} - \hat{\boldsymbol{i}} \tag{24}$$

where the correction term $\boldsymbol{f}(\cdot)$ or its filtered version serves as the emf estimate, as shown in Fig. 9. In this DO, the active emf $\boldsymbol{e}_{\mathrm{A}}$ is treated as a disturbance with assumed dynamics, and the correction $\boldsymbol{f}$ shall be modified accordingly when the assumed dynamics change. As shown in Fig. 10, the PI correction assumes $\boldsymbol{e}_{\mathrm{A}}$ is constant, the proportional-resonant (PR) correction assumes $\boldsymbol{e}_{\mathrm{A}}$ is sinusoidal with an angular speed of $\hat{\omega}$, and the SM correction in Fig. 10c/d assumes $\boldsymbol{e}_{\mathrm{A}}$ is bounded (and the bound is known).

To our interest, we shall introduce a general form of the dynamic correction function $f_\alpha(s) \in \mathbb{R}$ for $\alpha$-axis as follows

$$f_\alpha(s) = k_1|\tilde{i}_\alpha|^{\kappa_1}\mathrm{sign}(\tilde{i}_\alpha) + k_2\int |\tilde{i}_\alpha|^{\kappa_2}\mathrm{sign}(\tilde{i}_\alpha)\mathrm{d}t \tag{25}$$

The correction $f_\alpha$ is said to be *non-dynamic* if $k_2 = 0$ and said to be *dynamic* if $k_2 > 0$. "Dynamic" means $f_\alpha$ has internal state. In fact, since the integral term in (25) can be considered as an "extended state", the DO with dynamic correction is also called extended state observer (ESO). If $\kappa_1 < 1$, the correction is nonlinear function of $\tilde{i}_\alpha$, causing undesired dither in emf estimate, known as chattering.

*1) Linear DO:* From (25), assuming constant emf disturbance $s\boldsymbol{e}_{\mathrm{A}} = \boldsymbol{0}$ and putting $\kappa_1 = \kappa_2 = 1$, result in linear DO. In [77], non-dynamic correction is implemented. In [78], dynamic PI correction is used. The linear DO is deemed to be poorly damped if constant correction gains $k_1, k_2$ are used [5]. Frequency domain formulation of the DO with PI correction is proposed in [79], which is further generalized for salient PM motors in [69].

The constant emf assumption $s\boldsymbol{e}_{\mathrm{A}} = \boldsymbol{0}$ is not true [see (19b)], but it becomes reasonable if one transforms (24) into $dq$-frame, such that $dq$-frame emf is modelled as dc disturbance and the correction $\boldsymbol{f}$ becomes $\boldsymbol{Pf}$. In [80]–[82], $\boldsymbol{Pf}$ is implemented as a PI regulator. In [83], classical DO form (22) with LPF is used to estimate extended emf $\boldsymbol{e}_{\mathrm{E}}$ in $dq$-frame[2]. Note speed dependency is introduced in $dq$-frame linear DO.

*2) SMDO:* The working principle of SMDO is to use the correction term $\boldsymbol{f}$ to force $\hat{\boldsymbol{i}}$ to track $\boldsymbol{i}$. To make this happen, the norm of $\boldsymbol{f}$ should be larger than that of $\boldsymbol{e}_{\mathrm{A}}$ no matter how small the output error $\tilde{\boldsymbol{i}}$ is. For example, the classical SMDO uses a non-dynamic *SM control law*: $\boldsymbol{f} = k_1\mathrm{sign}(\boldsymbol{S})$ with simple *SM surface* $\boldsymbol{S} = \tilde{\boldsymbol{i}}$ and constant *SM gain* $k_1$, such that the norm $\|\boldsymbol{f}\|$ equals to $k_1$ as long as $\tilde{\boldsymbol{i}} \neq 0$. Since $||\boldsymbol{e}_{\mathrm{A}}||$ is proportional to $\omega$, and to assure a wide operating speed range, large SM gain $k_1$ is mandatory, implying DO performance varies as operating speed changes.

By using large but constant SM gain $k_1$, SMDO is speed-independent, but there are excessive noises in the "raw" estimated emf disturbance $\boldsymbol{f}$, known as chattering issues. To mitigate the chattering, it is proposed to use "milder" SM control law than the discontinuous correction $\mathrm{sign}(\cdot)$, such as saturation function [84], and sigmoid function [85]–[87]. Another idea is to design $\boldsymbol{f}$ as a linear combination of SM correction and proportional correction

[2]The analysis in [83] is in $\gamma\delta$-frame but the implementation is in $dq$-frame. For an example of $\gamma\delta$-frame observer implementation, see [64, Eqs. (17)].

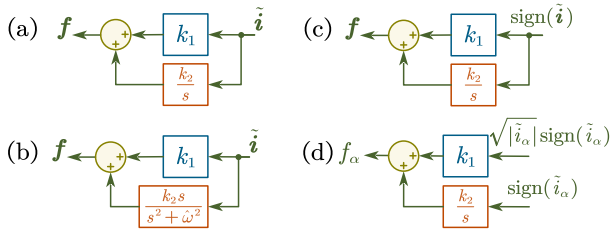


Fig. 10. Example correction function $\boldsymbol{f}$ used in disturbance observer. (a) PI, (b) PR, (c) discontinuous SM, and (d) continuous SM correction.

[84], [87]. However, those "milder" SM control laws break the Lyapunov stability of SMDO.

Alternatively, without modifying the SM control law, an additional LPF can be applied to $\boldsymbol{f}$, before $\hat{\theta}_d$ is extracted. The phase delay caused by the LPF should be compensated for different speeds [88]–[90]. Given a constant SM gain, it is suggested that the pole of the LPF should rely on $\hat{\omega}$ [84], as indicated in Fig. 9.

To avoid speed-dependency, it is recommended to implement $\boldsymbol{f}$ as a dynamic correction that puts signum inside an integral like the $k_2$ term in (25). This integral introduces an additional state, resulting in a second-order SMDO, and the newly introduced state can be interpreted as an estimate of the emf appearing in the current dynamics. For example, the super-twisting algorithm can be used to estimate the emf [91]–[93] [94, Sec. V], and the resulting *continuous* $\alpha$-axis correction is $f_\alpha = k_1|\tilde{i}_\alpha|^{\frac{1}{2}}\mathrm{sign}(\tilde{i}_\alpha) + k_2\int \mathrm{sign}\left(\tilde{i}_\alpha\right)\mathrm{d}t$, where the integral term serves as a continuous estimate of the emf, as shown in Fig. 10d. As a comparison, the second-order SMDO proposed in [95] uses *discontinuous* $\alpha$-axis correction as $f_\alpha = k_1\mathrm{sign}(\tilde{i}_\alpha) + k_2\int \mathrm{sign}\left(\tilde{i}_\alpha\right)\mathrm{d}t$, as shown in Fig. 10c. Note the continuity of $f_\alpha$ is decided by the $k_1$ term, and also note applying variable gain $k_1|\tilde{i}_\alpha|^{\frac{1}{2}}$ to $\mathrm{sign}(\tilde{i}_\alpha)$ does not eliminate chattering because the derivative of $|\tilde{i}_\alpha|^{\frac{1}{2}}$ is infinite when $\tilde{i}_\alpha = 0$. The chattering is reduced because of using smaller $k_1$ value and a nonzero $k_2$ term (that takes advantage of the history of output error $\tilde{\boldsymbol{i}}$).

So far, all SMDOs reviewed above use current error $\tilde{\boldsymbol{i}}$ as the SM surface $\boldsymbol{S}$. Improvement is expected by further designing SM surface. For example, SM surface involving the integral of current error $\int\tilde{\boldsymbol{i}}\mathrm{d}t$ can eliminate the reaching phase [96]–[98] [99, p.287]. SM surfaces involving the derivative of current error $s\tilde{\boldsymbol{i}}$ promise "convergence in finite time", such as the fast terminal SM manifold [100] and the non-singular terminal SM manifold [89]. Note the derivative can be reconstructed by super-twisting algorithm [89].

Besides, the SM gain can be designed to be a function of $\boldsymbol{S}$ [98], which is also known as the reaching law design. A less common idea to reduce SM gain is to execute the numerical integral of SMDO at a frequency that is three times as high as the pulse-width modulation (PWM) frequency [88], [101].

While most SMDO designs are speed-independent, it is possible to introduce speed dependency. First, similar to $dq$-frame linear DO, one can implement SMDO in $dq$-frame, and the $dq$-frame correction $\boldsymbol{Pf}$ in [102] is implemented as a combination of proportional correction and SM correction. Second, in [103], in addition to the dynamic correction $\boldsymbol{Pf}$, a speed-dependent SM surface that consists of current error and its integral is further selected. Third, the SMDO in [104] is designed based on the speed-dependent output equation of the extended emf model (37a). Finally, there are also examples of using speed-dependent tuning for second-order SMDO [93, (10)].

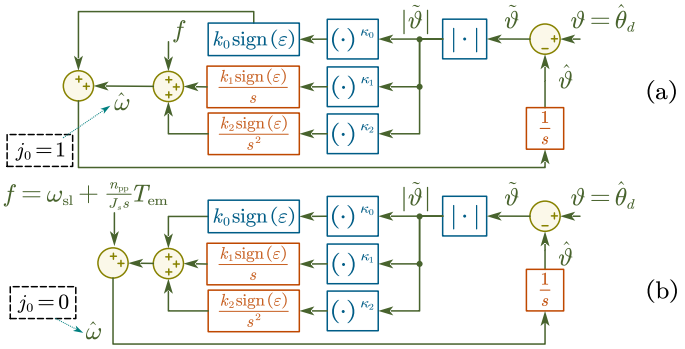


Fig. 11. The same 3rd-order position observer that generates two different rotor speed estimates. (a) Luenberger observer and (b) PID-like acceleration ($s\hat{\omega}$).

## IV. Separate Speed Estimation

This section focuses on DTC or DFO controlled drive, such that torque estimation is already done, and an estimate of some unknown state $(\hat{\boldsymbol{e}}_{\rm X}, \hat{\boldsymbol{\psi}}_{\rm A}, \hat{\theta}_d)$ is available. This estimate serves as the reference input (denoted by $\boldsymbol{\vartheta}$ or $\vartheta$) to the *separate* speed estimation. "Separate" means the speed estimation design assumes the reference input signal is independent of the speed estimate, i.e., it is *inherently sensorless* [45], neglecting speed error's influence on reference input.

### A. Direct Calculation

Steady state dynamics can be used to directly calculate speed, which provides a static but instantaneous speed estimate.

*1) Direct Calculation from Emf:* Speed is simply the emf amplitude divided by the flux amplitude [89], [91]. Note this direct calculation motivates the CM estimator (16).

*2) Direct Calculation from Position:* Speed estimate can be calculated by the forward difference of the flux angle $\hat{\theta}_d$ [10], [13]. An additional LPF is embedded to reduce the amplified noise [13].

*3) Direct Calculation from Flux Orthogonality:* Multiplying $-(\boldsymbol{J}\hat{\boldsymbol{\psi}}_s)^{\mathsf{T}}$ to both sides of the steady-state dynamics $s\hat{\boldsymbol{\psi}}_s = \hat{\omega}\boldsymbol{J}\hat{\boldsymbol{\psi}}_s$ gives a speed estimate: $\hat{\omega}(\hat{\boldsymbol{\psi}}_s^{\mathsf{T}}\hat{\boldsymbol{\psi}}_s) = -(\boldsymbol{J}\hat{\boldsymbol{\psi}}_s)^{\mathsf{T}} s\hat{\boldsymbol{\psi}}_s$, where the derivative $s\hat{\boldsymbol{\psi}}_s$ can be substituted by the forward difference of flux [105], or the calculated stator emf as $\boldsymbol{e}_s = \boldsymbol{u} - R\boldsymbol{i}$ [44], [106], or the voltage/emf estimate by SMDO [100], [107]–[111].

### B. General Observer for Speed

Assuming a scalar reference signal denoted as $\vartheta \triangleq \hat{\theta}_d$ is available from prior flux/emf estimation, then the following $(n+1)$-th order general state observer for $\vartheta$ summarizes a wide class of speed estimation methods:

$$
\begin{aligned}
s\hat{\vartheta} &= f(\vartheta) + \sum_{j=0}^{n} k_j \frac{|\tilde{\vartheta}|^{\kappa_j}\,{\rm sign}(\tilde{\vartheta})}{s^j}, \quad \text{with } k_j, \kappa_j \geq 0 \\
f(\vartheta) &= \omega_{\rm sl} + \tfrac{n_{\rm pp}}{sJ_s} T_{\rm em}
\end{aligned}
\tag{26}
$$

where the output error is $\tilde{\vartheta} = \vartheta - \hat{\vartheta}$. Similar generalization like (26) has been studied in literature, known as generalized PI observer (GPIO) [112] or generalized ESO (GESO) [113].

The position observer (26) does not define a speed estimate, and there are potentially $n+1$ variants of speed estimates [114]:

$$
\hat{\omega}_{j_0} = f(\vartheta) + \sum_{j=j_0}^{n} k_j \frac{|\tilde{\vartheta}|^{\kappa_j}\,{\rm sign}(\tilde{\vartheta})}{s^j} \text{ with } j_0 = 0, 1, 2, ..., n \tag{27}
$$

Table I gives a list of example implementations of (26). Fig. 11 shows block diagrams of (26) and (27) when $n=2,\ j_0=0,1$.

*1) State Observer Variants:* Position state observer (26) often uses motion equation (1) to render an inertia dependent $f(\vartheta)$ term. Linear corrections ($\kappa_j = 1$) are used in Luenberger observers [64], [80], [115], [116] [117, Fig. 9] and ESOs [90], [118], but ESO also allows nonlinear corrections [119], [120].

Alternatively, one can design a state observer for $q$-axis current by redefining $\vartheta$ and $f$ in (26) accordingly, for either PM motors [18] or induction motors [106]. Such scalar output observer can be considered as a reduced-order implementation of the original natural observer [121], or it can be understood as an ELO implementation of the $q$-axis current observer [61]. The difference is that the natural observer for $\vartheta = i_q$ utilizes motor's active power error $|u_q|\tilde{i}_q$ as output error, which, however, makes observer tuning to be dependent on $q$-axis voltage $u_q$ thus time-varying [18].

*2) Phase-Locked Loop (PLL):* PLL is widely used for extracting frequency information from $d$-axis angle error. During formulation of PLL, various types of position error signals can be exploited, such as the $q$-axis voltage [48], the angle of $\gamma\delta$-frame extended emf [81], $d$-axis current error [61], and the forward difference of high frequency components of $\alpha\beta$-frame current [116]. PLL for induction motors would need to add an additional slip relation [45] such that $f(\vartheta) = \omega_{\rm sl}$. Speed error during speed transients is inevitable because typical PLL is 2nd-order system that assumes constant speed [122], which is known as a type-2 system [37]. The transfer function from actual position to estimated position can be found in [83, Eq. (18)] and [81, Eq. (39)]. The PLL speed error during speed transients is analyzed in [78]. In [26], an additional PI term driven by torque error is further added to the PLL based speed estimate. PLL can be generalized for higher order to track time-varying speed [66, Eq. (24)], and see also [30] and [83, Eq. (22)] for an application of type-3 PLL for tracking ramp speed signal.

*3) Extended Kalman Filter (EKF):* In [71], [72], EKF is applied to a 3rd-order system with position, speed and acceleration as states, without needing inertia parameter $J_s$. This EKF is similar to type-3 PLL but has time-varying gains.

### C. Model Reference Adaptive System (MRAS)

Two different concepts of MRASs are shown in Fig. 12. Fig. 12a shows an MRAS whose reference and adjustable model

TABLE I
Examples of the General Position and Speed State Observer (26)

| Speed estimation | Order $n$ | Gain design | Alternative names | Assumed motion dynamics |
|---|---|---|---|---|
| Linear correction | 2 | Const. ($k_2=0$) | PLL, Adaptive system | $\omega_r = \text{Const.}$, $f = \omega_{\rm sl}$ |
| $\kappa_0 = 1$ | 3 | Const. | Generalized PLL | $\omega_r = kt$, $f = \omega_{\rm sl}$ |
| $\kappa_1 = 1$ | 3 | Time-varying | EKF, ELO | $\omega_r = kt$, $f = \omega_{\rm sl}$ |
| $\kappa_2 = 1$ | 3 | Const. | Speed observer, LESO, PI observer | $T_L = \text{Const.}$, $f = \omega_{\rm sl} + \frac{n_{\rm pp}}{sJ_s}T_{\rm em}$ |
| ... | 4 | Const. | Generalized LESO, Generalized PI observer | $T_L = kt$, $f = \omega_{\rm sl} + \frac{n_{\rm pp}}{sJ_s}T_{\rm em}$ |
| Nonlinear correction | 1 | Const. ($k_1=k_2=0$) | 1st-order SMDO ($\kappa_0=0$) | $\omega$ is bounded |
| $\exists j \in \{0,1,2\}$ | 2 | Const. ($k_2=0$) | 2nd-order SMDO ($\kappa_0=\frac{1}{2}, \kappa_1=0$) | $T_L$ is bounded |
| s.t. $\kappa_j \neq 1$ | 3 | Const. | Nonlinear ESO ($\kappa_0=1, \kappa_1=\frac{1}{2}, \kappa_2=\frac{1}{4}$) | $T_L = \text{Const.}$, $f = \omega_{\rm sl} + \frac{n_{\rm pp}}{sJ_s}T_{\rm em}$ |

PLL: phase locked loop. EKF: extended Kalman filter. LESO: linear extended state observer. ELO: extended Luenberger observer.

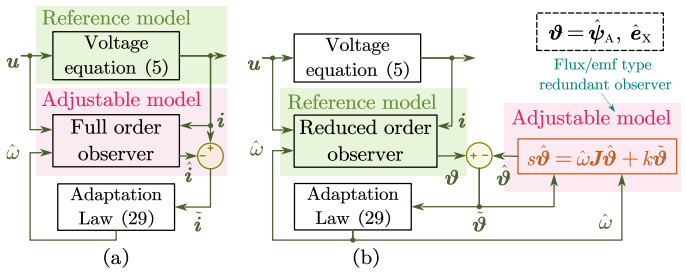


Fig. 12. MRAS with (a) full-order observer as adjustable model; (b) reduced-order observer as reference model and redundant observer as adjustable model. The key difference between the two examples of MRAS is whether its reference model exhibits explicit dependency on speed estimate $\hat{\omega}$.

are respectively the actual motor and the speed-adaptive full-order state observer. Fig. 12b shows an MRAS whose reference and adjustable model are respectively the reduced-order state observer and a speed-adaptive redundant observer.

*1) Redundant Observer:* Assuming an accurate estimate of the unknown states, denoted by $\vartheta$ (recall $\vartheta = \hat{\boldsymbol{e}}_X, \hat{\psi}_A$), is available, a redundant observer reconstructs the estimate only for extracting speed information from $\vartheta$ via an adaptation law. Redundant observer is corrected by the mismatch $\tilde{\vartheta} \triangleq \vartheta - \hat{\vartheta}$:

$$s\hat{\vartheta} = \hat{\omega}\boldsymbol{J}\hat{\vartheta} + k(\vartheta - \hat{\vartheta}) \quad \text{with } \vartheta = \hat{\psi}_A,\ \hat{\boldsymbol{e}}_A,\ \hat{\boldsymbol{e}}_E \tag{28}$$

Fig. 12b shows how the redundant observer is used as an adjustable model in MRAS, including the emf-type [69], [76], [77], [86], [87], [97], [98], and the flux-type [65].

*2) Speed Adaptation Law:* Adaptation law for field speed is

$$\hat{\omega} = \mathrm{PI}(s) \times \text{Regressor} \times \text{Output error} \tag{29}$$

where the output error can be the current error $\tilde{\boldsymbol{i}}$ from full-order observer (Fig. 12a), the flux/emf mismatch $\tilde{\vartheta}$ from redundant observer (Fig. 12b), or any other mismatch, e.g., the active flux amplitude mismatch $\varepsilon$ in (10b) [62]. Speed adaptation assumes speed is a constant parameter, but an inertia-dependent speed-adaptation law that includes an additional torque term is also proposed [61], [63], [105]. The selection of the regressor is critical and it often depends on how speed appears in the adopted model: example choices include active flux [9] and extended emf [68]. It is shown in [62] that decoupling of analysis between flux estimation and speed estimation is achieved via linearized model based observer tuning and wise selection of speed regressor. However, the fact is that the generation of speed regressor offers a degree-of-freedom to possibly find Lyapunov function, hence eliminating the need of linearization, which will be reviewed in the next section.

## V. Lose the Constant $\psi_A$ Assumption

As per (4a), $\psi_A$ is time-varying as long as $(L_d - L_q)i_d$ varies, and a change in $\psi_A$ leads to unmodelled dynamics $\boldsymbol{E}_u$ in (7a) and (19b), which will affect the performance of state observer as well as any other method relying on constant $\psi_A$ assumption. In practice, time-varying $\psi_A$ could be beneficial for improving operating efficiency or dynamic performance. For example, at high speeds, faster speed dynamic process can be achieved if the flux amplitude is first weakened such that more dc bus voltage becomes available for producing torque current [123].

For PM motors, the strategy is mainly to compensate the unmodelled dynamics. In [11], an angle compensation that takes into account the unmodelled dynamics in (19b) when $\psi_A$ varies is proposed. In [9], the $si_d$ in the unmodelled dynamics $\boldsymbol{E}_u$ in (7a) is compensated by its estimate.

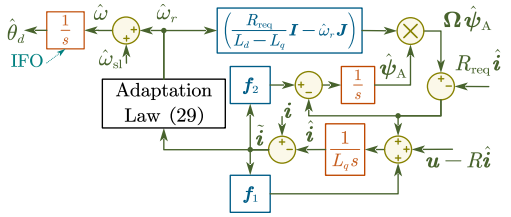


Fig. 13. Adaptive full-order observer for induction motor model (31).

For induction motors, the voltage $\boldsymbol{E}_u$ is closely related to the voltage drop on the rotor resistance, and hence it can, in fact, be modelled. This section is dedicated for induction motors.

### A. Induction Motor Model with Time-Varying $\psi_A$

For induction motors, the unmodelled dynamics $\boldsymbol{E}_u$ satisfy

$$\boldsymbol{E}_u = \boldsymbol{P}^{-1}(\theta_d)\begin{bmatrix} s\psi_A \\ 0 \end{bmatrix} \overset{(4a)}{=} -R_{req}\underbrace{\left(\frac{\boldsymbol{\psi}_A}{L_d - L_q} - \boldsymbol{i}\right)}_{\text{the rotor current}} - \omega_{sl}\boldsymbol{J}\boldsymbol{\psi}_A \tag{30}$$

in which (4a) and (3) have been substituted, and from which the slip relation $\omega_{sl} = \frac{R_{req} i_q}{\psi_A}$ is derived. The model with stator current and active flux as states is derived from (5), (7a) and (30):

$$L_q s\boldsymbol{i} = \boldsymbol{u} - R\boldsymbol{i} - s\boldsymbol{\psi}_A \tag{31a}$$

$$s\boldsymbol{\psi}_A = R_{req}\boldsymbol{i} + \tfrac{-R_{req}}{L_d - L_q}\boldsymbol{\psi}_A + (\omega - \omega_{sl})\,\boldsymbol{J}\boldsymbol{\psi}_A \tag{31b}$$

$$\triangleq R_{req}\boldsymbol{i} - \boldsymbol{\Omega}\boldsymbol{\psi}_A \tag{31c}$$

which is exactly the inverse-$\Gamma$ circuit induction motor model, with active flux $\boldsymbol{\psi}_A$ being equivalent to the rotor flux, $L_d$ denoting stator inductance, $L_q$ designating transient leakage inductance, and $\boldsymbol{\Omega} \triangleq \frac{R_{req}}{L_d - L_q}\boldsymbol{I} - \omega_r\boldsymbol{J}$. There are two facts that make induction motors unique:

1) Active flux amplitude $\psi_A$ is not constant and is maintained by stator excitation for non-PM motors.
2) There is a slip speed $\omega_{sl}$ difference between field speed $\omega$ and rotor speed $\omega_r$, i.e., $\omega_r = \omega - \omega_{sl}$.

In other words, the induction motor is not a PM motor nor synchronous motor. These two facts correspond to the two unique features of sensorless induction motors:

1) There is a chance for estimated flux amplitude $\hat{\psi}_A$ to collapse [124]. There is also a chance for a change in flux amplitude being mis-interpreted as a change in flux angle, which is revealed in the "basic relations for sensorless flux estimation" [45, Eq. (13)]. As a result, unstable sensorless operation that is not observed in PM motors might happen (e.g., at low speed regenerating operation).
2) Zero speed operation under load does not mean zero frequency operation for induction motors.

### B. The Common Act of Choosing Active Flux as State

Many researches have been devoted for achieving speed estimation using the model (31). Note the estimated flux is seldom used for Park transformation, and in most cases, the IFO $d$-axis angle $\frac{1}{s}\hat{\omega}$ is used to define the $dq$-frame of an induction motor.

*1) State Observer Design Attempts:* Using (31), speed-adaptive observer can be designed in $\alpha\beta$-frame [67], [105], [125]–[131] or $dq$-frame [63], [132]. Linear correction is widely used, but SM correction can also be used [67], [105], [130]. Fig. 13 shows a typical implementation. Time-varying correction functions are used in EKF and ELO, where speed is treated as an extended state so that linearization is required [133, Sec. 4.5.3.5].

For better dynamic performance, $\omega_r$ is further treated as observer state in $dq$-frame SM state observer [134] with $d$-axis

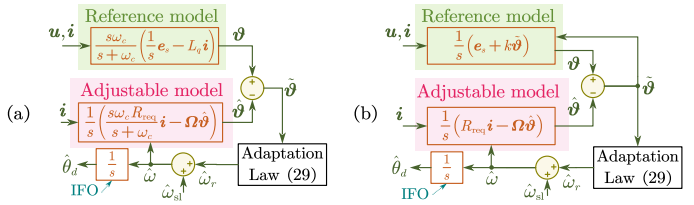


Fig. 14. Flux type MRAS for IFO of sensorless induction motor, where the VM is stabilized by (a) the HPF $\frac{s\omega_c}{s+\omega_c}$, or (b) the mismatch $\tilde{\boldsymbol{\vartheta}}$. Note reference model has no explicit speed dependency (cf. Fig. 12b).

current error chosen as output error. A different approach, however, is to put all the correction terms into the dynamics of the load torque estimate $\hat{T}_L$ and uses an exact copy of motor dynamics (31) and (1) to establish a so-called natural observer [121].

*2) Stability Challenges at Low Speed Regeneration:* It is quite a challenge to stabilize the full-order state observer for (31) in low speed regeneration even when speed is observable. Classical designs are flawed. For example, the stable speed adaptation law derived from Lyapunov function [127] depends on the unknown flux error; and the hyper-stability analysis in [125] depends on the assumption that the ratio between flux error norm and current error norm has finite upper bound (so that the unknown flux error can be replaced by current error). Careful observer gain designs based on the linearized model (see, e.g., [128], [131], [135], [136]) and the positive real property [137] are proposed for extending stable operating region. Alternatively, it is also effective to re-design the speed adaptation law [129], [138], [139] [140, Eq. (26)]. Readers are referred to [141] for a survey of the stabilization methods.

*3) MRAS:* In the field of sensorless induction motor drive, MRAS is a jargon for a system with the VM (5) being reference model and the new CM (31c) being adjustable model. The pioneer work on MRAS in [42] (see also the follow-up works [142], [143]) chooses VM estimator in (14) as reference model, and implement CM with high-pass filtered $\boldsymbol{i}$ as adjustable model, as shown in Fig. 14a. As a result, the obtained flux estimate has significant delays with respect to the actual flux thus it cannot be used for DFO. This is a good example showing the spirit of the IFO nature of sensorless induction motors, that an accurate estimate of flux/emf is not needed, because the IFO $d$-axis angle estimate only depends on the speed estimate. However, there are also attempts to compensate the gain and lag introduced in (14) [144].

Alternatively, one can stabilize VM estimator using the mismatch $\tilde{\boldsymbol{\vartheta}}$ between outputs of VM and CM estiamtors as correction. Fig. 14b shows an example of proportional correction $k\tilde{\boldsymbol{\vartheta}}$. [145]. The MRAS implementation in [19] has made it clear that the amplitude mismatch is used to stabilize VM estimator, while the angle mismatch is used to tune $\hat{\omega}$ used in CM estimator. In [146], the VM is transformed to an estimated $dq$-frame to derive a generalized slip relation in terms of the VM correction gains. The dual reference observer proposed in [147] is also an MRAS, and is an example of implementing the amplitude correction (11) in its current error form (10b) in a time-varying $\psi_{\mathrm{A}}$ model. In [143], the speed adaptation law is implemented as an SM control law. In [148], the correction in VM is replaced with a super-twisting based dynamic correction. Readers are referred to [149] for a dedicated review of MRAS variants having different choices of output errors.

### C. State Observer Design via Change of States

To attack the regeneration instability challenge, an ideal solution is to find a globally stable speed-adaptive observer design. In the classics of adaptive observer design [150]–[152], stable observer design is often proposed for a class of state-affine systems, which do not describe the induction motor dynamics (31). In fact, it has been shown in [153] that in order to find a Lyapunov function for the full-order state observer with $(\boldsymbol{i}, \boldsymbol{\psi}_{\mathrm{A}})$ as states, the observer coefficients must be dependent on the actual speed, implying globally stable design does not exist. Thus to obtain global stability, one needs to either find a proper state transformation that can describe the induction motor as a system in the *adaptive observer form* [151]

$$s\begin{bmatrix}\boldsymbol{i}\\ \boldsymbol{x}\end{bmatrix}=\begin{bmatrix}\boldsymbol{0} & \boldsymbol{I}\\ \boldsymbol{0} & \boldsymbol{0}\end{bmatrix}\begin{bmatrix}\boldsymbol{i}\\ \boldsymbol{x}\end{bmatrix}+\boldsymbol{\Phi}(\boldsymbol{i},\boldsymbol{u})\omega_r+\boldsymbol{\Phi}_0(\boldsymbol{i},\boldsymbol{u}) \tag{32}$$

where $\boldsymbol{\Phi}\in\mathbb{R}^4$ is the regressor of speed that consists of only known signals $(\boldsymbol{i},\boldsymbol{u})$, and $\boldsymbol{x}$ is the new unknown state; or develop advanced observer design applicable to a wider class of systems that allow unknown speed regressor $\boldsymbol{\Phi}(\boldsymbol{x})$ [154], [155].

*1) Change of States:* A list of state transformations for induction motors is given in Table II. Model 1 is (31). Integrator backstepping based observer design is proposed for model 2 ($\boldsymbol{x}=\boldsymbol{e}_{\mathrm{A}}$) in [94, Sec. III], where speed is assumed as a known signal in the stability proof. In [140], an attempt to apply adaptive observer design proposed in [150] to model 3 ($\boldsymbol{x}=-\boldsymbol{e}_{\mathrm{A}}$) has ended with requiring infinite gain to attain asymptotical stability, where the signal $s\boldsymbol{i}$ is obtained using a state variable filter—which can be avoided if model 4 ($\boldsymbol{x}=\boldsymbol{\Omega}\boldsymbol{\psi}_{\mathrm{A}}$) is used instead [140]. The research using model 5 ($\boldsymbol{x}=\boldsymbol{\psi}_s$) is summarized in the monograph [156], and the key property of choosing stator flux as the unknown internal state is that there is no unknown variable $\omega_r$ appearing in the dynamics of unknown state $\boldsymbol{x}$. Finally, model 6 ($\boldsymbol{x}=\boldsymbol{\Omega}\boldsymbol{\psi}_s$) is in adaptive observer form (32) and therefore, the existence of globally stable speed-adaptive observer for induction motor is an established fact [157]–[159], where filtering the original speed regressor is found essential [159].

*2) Advances in High Gain Observer Design:* The advances in high-gain observer (HGO) design [154], [155] accept a wider class of systems than (32), and application of this HGO to model 6 is studied in [160]. Moreover, the speed $\omega_r$ and load torque $T_L$ can be treated as states, so that model 4 has been extended with an third $\mathbb{R}^2$ state as $\boldsymbol{z}=-s(\omega_r\boldsymbol{J}\boldsymbol{\psi}_{\mathrm{A}})$ [161]. The requirement on the partitioned matrix needed in [154], [161] is later removed in [155], which allows one to design HGO in terms of the two scalar states $\omega_r$ and $T_L$ instead of the $\mathbb{R}^2$ vector $\boldsymbol{z}$ [155]. Note the speed regressor redesign from [152] has facilitated the above Lyapunov stability based HGO design [154], [155].

TABLE II
LIST OF STATE TRANSFORMATIONS FOR INDUCTION MOTORS ASSUMING CONSTANT SPEED

| Model No. | Output state dynamics | Unknown state | Unknown state dynamics | Speed regressor $\boldsymbol{\Phi}$ |
|---|---|---|---|---|
| 1 | $L_q s\boldsymbol{i}=-s\boldsymbol{x}+\boldsymbol{u}-R\boldsymbol{i}$ | $\boldsymbol{x}=\boldsymbol{\psi}_{\mathrm{A}}$ | $s\boldsymbol{x}=-\boldsymbol{\Omega}\boldsymbol{x}+R_{\mathrm{req}}\boldsymbol{i}$ | $[(-\boldsymbol{J}\boldsymbol{x})^{\mathsf{T}},(\boldsymbol{J}\boldsymbol{x})^{\mathsf{T}}]^{\mathsf{T}}$ |
| 2 | $L_q s\boldsymbol{i}=-\boldsymbol{x}+\boldsymbol{u}-R\boldsymbol{i}$ | $\boldsymbol{x}=\boldsymbol{e}_{\mathrm{A}}$ | $s\boldsymbol{x}=-\boldsymbol{\Omega}\boldsymbol{x}+R_{\mathrm{req}}s\boldsymbol{i}$ | $[\boldsymbol{0},(\boldsymbol{J}\boldsymbol{x})^{\mathsf{T}}]^{\mathsf{T}}$ |
| 3 | $L_q s\boldsymbol{i}=\boldsymbol{x}+\boldsymbol{u}-R\boldsymbol{i}$ | $\boldsymbol{x}=-\boldsymbol{e}_{\mathrm{A}}$ | $s\boldsymbol{x}=-\boldsymbol{\Omega}\boldsymbol{x}-R_{\mathrm{req}}s\boldsymbol{i}$ | $[\boldsymbol{0},(\boldsymbol{J}\boldsymbol{x})^{\mathsf{T}}]^{\mathsf{T}}$ |
| 4 | $L_q s\boldsymbol{i}=\boldsymbol{x}+\boldsymbol{u}-(R+R_{\mathrm{req}})\,\boldsymbol{i}$ | $\boldsymbol{x}=\boldsymbol{\Omega}\boldsymbol{\psi}_{\mathrm{A}}$ | $s\boldsymbol{x}=-\boldsymbol{\Omega}\,(\boldsymbol{x}-R_{\mathrm{req}}\boldsymbol{i})$ | $[\boldsymbol{0},(\boldsymbol{J}(\boldsymbol{x}-R_{\mathrm{Req}}\boldsymbol{i}))^{\mathsf{T}}]^{\mathsf{T}}$ |
| 5 | $L_q s\boldsymbol{i}=\boldsymbol{\Omega}\,(\boldsymbol{x}-L_q\boldsymbol{i})+\boldsymbol{u}-(R+R_{\mathrm{req}})\,\boldsymbol{i}$ | $\boldsymbol{x}=\boldsymbol{\psi}_s$ | $s\boldsymbol{x}=\boldsymbol{u}-R\boldsymbol{i}$ | $[(-\boldsymbol{J}(\boldsymbol{x}-\boldsymbol{L}_q\boldsymbol{i}))^{\mathsf{T}},\boldsymbol{0}]^{\mathsf{T}}$ |
| 6 | $L_q s\boldsymbol{i}=\boldsymbol{x}+\boldsymbol{u}-\left(\frac{L_d R_{\mathrm{req}}}{L_d-L_q}+R\right)\boldsymbol{i}+\omega_r\boldsymbol{J}L_q\boldsymbol{i}$ | $\boldsymbol{x}=\boldsymbol{\Omega}\boldsymbol{\psi}_s$ | $s\boldsymbol{x}=\boldsymbol{\Omega}\,(\boldsymbol{u}-R\boldsymbol{i})$ | $[\boldsymbol{J}\boldsymbol{y},-\boldsymbol{J}(\boldsymbol{u}-R\boldsymbol{i})^{\mathsf{T}}]^{\mathsf{T}}$ |

Note: $\boldsymbol{\Omega}=\frac{R_{\mathrm{req}}}{L_d-L_q}\boldsymbol{I}-\omega_r\boldsymbol{J}$.

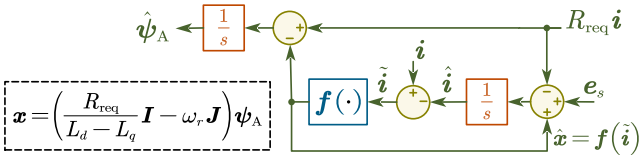


Fig. 15. SMDO design for induction motor that estimates the disturbance $\boldsymbol{x}$.

### D. Disturbance Observer Design via Change of States

Substituting (31c) into (31a) will introduce a disturbance variable denoted as $\boldsymbol{x} = \boldsymbol{\Omega}\boldsymbol{\psi}_{\mathrm{A}}$. Fig. 15 shows the general DO for estimating this disturbance, where SM correction is widely used [107]–[111], and linear dynamic correction is also studied [162]. Alternatively, one can design a full-order SMDO for model 1 or model 5 with the speed-dependent term $\omega_r\boldsymbol{J}\boldsymbol{\psi}_{\mathrm{A}}$ or $\omega_r\boldsymbol{J}\boldsymbol{\psi}_s$ being treated as disturbance [147].

## VI. Considerations for Low Speed Operations

The sufficient conditions for preserving ac motor observability provide guidance for stable operation near $s\theta_d = 0$. The state vector $[i_\alpha, i_\beta, \omega, \theta_d]^{\mathsf{T}}$ of a PM motor is locally weakly observable, if the following inequality holds [163]:

$$s\theta_d = \omega \neq s\tan^{-1}\left(\frac{L_d - L_q}{\psi_{\mathrm{A}}} i_q\right) \tag{33}$$

The state vector $[i_\alpha, i_\beta, \psi_{\alpha\mathrm{A}}, \psi_{\beta\mathrm{A}}, \omega, T_L]^{\mathsf{T}}$ of an induction motor is locally weakly observable, if the inequality holds [161], [163]:

$$\omega \neq s\tan^{-1}\left(\frac{L_d - L_q}{R_{\mathrm{req}}}\omega_r\right) = s\tan^{-1}\left(\frac{L_d - L_q}{R_{\mathrm{req}}}\omega - \frac{L_d - L_q}{\psi_{\mathrm{A}}} i_q\right) \tag{34}$$

where the slip speed has been substituted. To preserve the observability at $\omega = 0$, both (33) and (34) suggest that an auxiliary observability vector in $dq$-frame[3]

$$\boldsymbol{\psi}_{\mathcal{O}}^{dq} \triangleq \begin{bmatrix} \psi_{\mathrm{A}} \\ -(L_d - L_q)\, i_q \end{bmatrix} \tag{35}$$

should rotate or change its direction with respect to the $d$-axis. In particular, the local weak observability of a surface mounted PM motor holds with non-zero acceleration at $\omega = 0$, i.e., zero frequency crossing [164].

Slow speed reversal test has been recommended to test stability margin of a sensorless drive near zero frequency operation [141]. The CM estimator can survive the test with the help of the load-dependent $i_d$ excitation [50], where the $d$-axis angle error still shows trends of divergence during zero frequency crossing. It is suggested to use high frequency signal injection to assist zero frequency crossing for the $dq$-frame VM estimator in [35]. However, the $\alpha\beta$-frame VM estimator shows smooth $d$-axis angle waveform even during zero frequency crossing [18], [32], [37], [106] Note only voltage compensation is needed in [18], [32], [106], while the speed-dependent flux compensation is used in [37]. The SMDO proposed in [84] is also found to be able to perform the test, but shows increased noises in speed estimate as compared to its VM counterpart [18]. The globally stable speed-adaptive observer also shows speed divergence near zero frequency crossing because the persistency of excitation is lost at dc excitation [158]. Typical acceleration rate of the slow reversal is between 50–100 r/min/s, whereas a successful 5 r/min/s test is reported in [106], [158], and it can go down to 2 r/min/s if deliberate flux weakening is allowed [158]. As a final note, compared with operating at standstill (see, e.g., [18], [37]), operating extremely near zero frequency (e.g., 1 r/min [6]) is considered as a more challenging working condition.

[3]It is interesting to point out that this auxiliary flux vector is used to design a regressor for the speed adaptation law of the $dq$-frame VM estimator in [62].

## VII. Concluding Remarks

The act to use the same torque expression for all ac motors, provides us a unified perspective to review fundamental frequency sensorless algorithms based on the model of torque-producing flux, i.e., active flux. The resulting equivalent circuit models the effect of the PM, the saliency and the rotor conductors.

The torque estimation problem can be solved directly or indirectly, which corresponds to a DFO or IFO sensorless drive. The *direct* torque estimation includes the VM estimator and the observers, such that $d$-axis angle is computed from $\alpha\beta$ components of flux or emf vector. The *indirect* torque estimation problem is turned into speed estimation problem via the CM estimator. The CM estimator enables speed estimation in IFO $dq$-frame, but any other speed estimation method such as MRAS and speed-adaptive state observer can be used—which is often seen in IFO controlled induction motors.

No method is perfect. VM is critically stable, CM estimator has algebraic loop issues, state observer is disturbed by estimated speed error, and disturbance observer suffers from undesired dither in estimation. Nevertheless, advances to each method have been made in literature:

1) The VM estimator is analyzed in the $dq$ frame to derive operating speed dependent stability results [34], implying stability is guaranteed with speed dependent tuning.
2) The CM estimator is linearized for analysis, from which "complete stability" is attained with proper tuning [50], [165].
3) Challenges have been reported in designing stable state observer for model using active flux as states, while the researches that involve *change of states* are fruitful, e.g., globally stable speed-adaptive observer (except zero stator frequency condition) [12], [155], [158].
4) Dynamic SM correction of higher order has long been found able to eliminate chattering in SMDO (see e.g., [166, Ch. 6]).

Unlike IFO drive, a DFO drive needs to estimate speed *separately*. A general observer is proposed to summarize various speed estimation algorithms including PLL, ELO, EKF, GPIO, GESO, and SMDO, which differ in terms of linear or nonlinear corrections, time-invariant or time-varying gains, and their assumed motion dynamics. It is worth mentioning that for the same general observer of order $n$, there are potentially $n + 1$ variants of speed estimates having different characteristics in terms of dynamic performance and noise attenuation.

The applicability of sensorless algorithms depends. Speed estimation methods assuming constant speed are more suited for motors with large inertia, while high dynamic performance can be obtained with higher order speed estimation. For ultra-high speed applications with high switching frequencies, CM estimator is recommended for its minimum computational cost. For high-saliency motors and non-PM motors, as the active flux amplitude is regulated in real-time, designs that take into account of the dynamic active flux amplitude should be considered. For low speed applications, the local weak observability has suggested to adopt high saliency PM motor or induction motor from a theoretical point of view.

## Appendix A
## The History of Extended EMF Model

By manipulating inductance, the $dq$-model (6) is rewritten

$$\begin{aligned} s\psi_{\mathrm{PM}} + L_d s i_d &= u_d - Ri_d + \omega L_q i_q \\ \underbrace{\omega\psi_{\mathrm{A}} - (L_d - L_q)\tfrac{\mathrm{d}}{\mathrm{d}t} i_q}_{\text{Amplitude of the extended emf } \boldsymbol{e}_{\mathrm{E}}} + L_d s i_q &= u_q - Ri_q - \omega L_q i_d \end{aligned} \tag{36}$$

Transforming (36) to $\alpha\beta$-frame yields extended emf model: [76]

$$L_d s\boldsymbol{i} + \boldsymbol{e}_{\mathrm{E}} + \omega \boldsymbol{J}\left(L_d - L_q\right)\boldsymbol{i} = \boldsymbol{u} - R\boldsymbol{i} \tag{37a}$$

$$\text{with } s\boldsymbol{e}_{\mathrm{E}} = \omega \boldsymbol{J}\boldsymbol{e}_{\mathrm{E}} + \text{Unmodelled Dynamics} \tag{37b}$$

Historically, it is not easy to design sensorless algorithm for salient-pole PM motors, owing to the position-dependent inductance that leads to a highly nonlinear model. The salient-pole PM motor can be treated as a non-salient one if one assumes $\|(L_d - L_q)\boldsymbol{i}\| \ll \psi_{\mathrm{PM}}$ [76]. The idea of extended emf was timely proposed to relax the need of this low saliency assumption. Note the current dynamics are now explicitly dependent on $\omega$ in (37a).

## REFERENCES


[1] B.-H. Bae, S.-K. Sul, J.-H. Kwon, and J.-S. Byeon, "Implementation of sensorless vector control for super-high-speed pmsm of turbo-compressor," *IEEE Trans. Ind. Appl.*, vol. 39, no. 3, pp. 811–818, 2003.

[2] M. Pacas, "Sensorless drives in industrial applications," *IEEE Ind. Electron. Mag.*, vol. 5, no. 2, pp. 16–23, jun 2011.

[3] H. Mohan, M. K. Pathak, and S. K. Dwivedi, "Sensorless control of electric drives–a technological review," *IETE Technical Review*, vol. 37, no. 5, pp. 504–528, 2020.

[4] G. Wang, M. Valla, and J. Solsona, "Position sensorless permanent magnet synchronous machine drives—a review," *IEEE Trans. Ind. Electron.*, vol. 67, no. 7, pp. 5830–5842, 2020.

[5] C. J. V. Filho, D. Xiao, R. P. Vieira, and A. Emadi, "Observers for high-speed sensorless PMSM drives: Design methods, tuning challenges and future trends," *IEEE Access*, vol. 9, pp. 56 397–56 415, 2021.

[6] I. Boldea, M. C. Paicu, and G. Andreescu, "Active flux concept for motion-sensorless unified ac drives," *IEEE Trans. Power Electron.*, vol. 23, no. 5, pp. 2612–2618, 2008.

[7] G. R. Slemon, "Modelling of induction machines for electric drives," *IEEE Trans. Ind. Appl.*, vol. 25, no. 6, pp. 1126–1131, Nov 1989.

[8] R. Ortega, N. Barabanov, G. Escobar, and E. Valderrama, "Direct torque control of induction motors: stability analysis and performance improvement," *IEEE Trans. Autom. Control*, vol. 46, no. 8, pp. 1209–1222, Aug 2001.

[9] S. Koonlaboon and S. Sangwongwanich, "Sensorless control of interior permanent-magnet synchronous motors based on a fictitious permanent-magnet flux model," in *Fourtieth IAS Annual Meeting. Conference Record of the 2005 Industry Applications Conference, 2005.* IEEE, 2005.

[10] M. Hasegawa and K. Matsui, "Position sensorless control for interior permanent magnet synchronous motor using adaptive flux observer with inductance identification," *IET Electric Power Applications*, vol. 3, no. 3, p. 209, 2009.

[11] Y. Zhao, Z. Zhang, W. Qiao, and L. Wu, "An extended flux model-based rotor position estimator for sensorless control of salient-pole permanent-magnet synchronous machines," *IEEE Trans. Power Electron.*, vol. 30, no. 8, pp. 4412–4422, aug 2015.

[12] C. Verrelli, P. Tomei, E. Lorenzani, G. Migliazza, and F. Immovilli, "Nonlinear tracking control for sensorless permanent magnet synchronous motors with uncertainties," *Control Engineering Practice*, vol. 60, pp. 157–170, 2017.

[13] R. Wu and G. Slemon, "A permanent magnet motor drive without a shaft sensor," *IEEE Trans. Ind. Appl.*, vol. 27, no. 5, pp. 1005–1011, 1991.

[14] J. Holtz and J. Quan, "Drift- and parameter-compensated flux estimator for persistent zero-stator-frequency operation of sensorless-controlled induction motors," *IEEE Trans. Ind. Appl.*, vol. 39, no. 4, pp. 1052–1060, July 2003.

[15] J. Chen, J. Mei, X. Yuan, Y. Zuo, J. Zhu, and C. H. T. Lee, "Online adaptation of two-parameter inverter model in sensorless motor drives," *IEEE Trans. Ind. Electron.*, vol. 69, no. 10, pp. 9860–9871, 2022.

[16] M. Rahman, L. Zhong, M. Haque, and M. Rahman, "A direct torque-controlled interior permanent-magnet synchronous motor drive without a speed sensor," *IEEE Trans. Energy Convers.*, vol. 18, no. 1, pp. 17–22, 2003.

[17] J. Holtz and J. Quan, "Sensorless vector control of induction motors at very low speed using a nonlinear inverter model and parameter identification," *IEEE Trans. Ind. Appl.*, vol. 38, no. 4, pp. 1087–1095, Jul 2002.

[18] J. Chen, J. Mei, X. Yuan, Y. Zuo, and C. H. T. Lee, "Natural speed observer for nonsalient ac motors," *IEEE Trans. Power Electron.*, vol. 37, no. 1, pp. 14–20, Jan 2022.

[19] C. Lascu, I. Boldea, and F. Blaabjerg, "A modified direct torque control for induction motor sensorless drive," *IEEE Trans. Ind. Appl.*, vol. 36, no. 1, pp. 122–130, 2000.

[20] J.-H. Kim, J.-W. Choi, and S.-K. Sul, "Novel rotor-flux observer using observer characteristic function in complex vector space for field-oriented induction motor drives," *IEEE Trans. Ind. Appl.*, vol. 38, no. 5, pp. 1334–1343, 2002.

[21] A. Yoo and S.-K. Sul, "Design of flux observer robust to interior permanent-magnet synchronous motor flux variation," *IEEE Trans. Ind. Appl.*, vol. 45, no. 5, pp. 1670–1677, 2009.

[22] F. J. W. Barnard, W. T. Villet, and M. J. Kamper, "Hybrid active-flux and arbitrary injection position sensorless control of reluctance synchronous machines," in *2014 International Symposium on Power Electronics, Electrical Drives, Automation and Motion*. IEEE, jun 2014.

[23] H.-S. Kim, S.-K. Sul, H. Yoo, and J. Oh, "Distortion-Minimizing Flux Observer for IPMSM Based on Frequency-Adaptive Observers," *IEEE Trans. Power Electron.*, vol. 35, no. 2, pp. 2077–2087, Feb. 2020.

[24] C. Pitic, G.-D. Andreescu, F. Blaabjerg, and I. Boldea, "Ipmsm motion-sensorless direct torque and flux control," in *31st Annual Conference of IEEE Industrial Electronics Society, 2005. IECON 2005.*, 2005, pp. 1–6.

[25] C. Lascu and G.-D. Andreescu, "Sliding-mode observer and improved integrator with DC-offset compensation for flux estimation in sensorless-controlled induction motors," *IEEE Trans. Ind. Electron.*, vol. 53, no. 3, pp. 785–794, jun 2006.

[26] G.-D. Andreescu, C. Pitic, F. Blaabjerg, and I. Boldea, "Combined flux observer with signal injection enhancement for wide speed range sensorless direct torque control of IPMSM drives," *IEEE Trans. Energy Convers.*, vol. 23, no. 2, pp. 393–402, jun 2008.

[27] A. K. Jain and V. T. Ranganathan, "Modeling and field oriented control of salient pole wound field synchronous machine in stator flux coordinates," *IEEE Trans. Ind. Electron.*, vol. 58, no. 3, pp. 960–970, mar 2011.

[28] S.-C. Agarlita, I. Boldea, and F. Blaabjerg, "High-frequency-injection-assisted "active-flux"-based sensorless vector control of reluctance synchronous motors, with experiments from zero speed," *IEEE Trans. Ind. Appl.*, vol. 48, no. 6, pp. 1931–1939, 2012.

[29] A. Yousefi-Talouki, P. Pescetto, and G. Pellegrino, "Sensorless direct flux vector control of synchronous reluctance motors including standstill, MTPA, and flux weakening," *IEEE Trans. Ind. Appl.*, vol. 53, no. 4, pp. 3598–3608, jul 2017.

[30] H. Wang, Y. Yang, D. Chen, X. Ge, S. Li, and Y. Zuo, "Speed-sensorless control of induction motors with an open-loop synchronization method," *IEEE Trans. Emerg. Sel. Topics Power Electron.*, vol. 10, no. 2, pp. 1963–1977, 2022.

[31] T. Ohtani, N. Takada, and K. Tanaka, "Vector control of induction motor without shaft encoder," *IEEE Trans. Ind. Appl.*, vol. 28, no. 1, pp. 157–164, Jan 1992.

[32] G.-J. Jo and J.-W. Choi, "Rotor flux estimator design with offset extractor for sensorless-driven induction motors," *IEEE Trans. Power Electron.*, vol. 37, no. 4, pp. 4497–4510, 2021.

[33] J. Lee, J. Hong, K. Nam, R. Ortega, L. Praly, and A. Astolfi, "Sensorless control of surface-mount permanent-magnet synchronous motors based on a nonlinear observer," *IEEE Trans. Power Electron.*, vol. 25, no. 2, pp. 290–297, feb 2010.

[34] R. Ortega, L. Praly, A. Astolfi, J. Lee, and K. Nam, "Estimation of rotor position and speed of permanent magnet synchronous motors with guaranteed stability," *IEEE Trans. Control Syst. Technol.*, vol. 19, no. 3, pp. 601–614, 2011.

[35] A. Piippo, M. Hinkkanen, and J. Luomi, "Analysis of an adaptive observer for sensorless control of interior permanent magnet synchronous motors," *IEEE Trans. Ind. Electron.*, vol. 55, no. 2, pp. 570–576, 2008.

[36] M. X. Bui, M. F. Rahman, and D. Xiao, "A hybrid sensorless controller of an interior permanent magnet synchronous machine using current derivative measurements and a sliding mode observer," *IEEE Trans. Ind. Appl.*, vol. 56, no. 1, pp. 314–324, 2020.

[37] Y. Park and S. K. Sul, "Sensorless control method for pmsm based on frequency-adaptive disturbance observer," *IEEE Trans. Emerg. Sel. Topics Power Electron.*, vol. 2, no. 2, pp. 143–151, June 2014.

[38] J. Ji, Y. Jiang, W. Zhao, Q. Chen, and A. Yang, "Sensorless control of linear vernier permanent-magnet motor based on improved mover flux observer," *IEEE Trans. Power Electron.*, vol. 35, no. 4, pp. 3869–3877, apr 2020.

[39] Y. Zhang, Z. Yin, F. Gao, and J. Liu, "Research on anti-dc bias and high-order harmonics of a fifth-order flux observer for ipmsm sensorless drive," *IEEE Trans. Ind. Electron.*, vol. 69, no. 4, pp. 3393–3406, 2022.

[40] J. Zhang, J. Chai, X. Sun, and H. Lu, "An improved voltage model integral algorithm of induction motors based on the orthogonality between back emf and flux," *Transactions of China Electrotechnical Society*, vol. 29, no. 3, pp. 41–49, 2014.

[41] D. Stojić, M. Milinković, S. Veinović, and I. Klasnić, "Improved stator flux estimator for speed sensorless induction motor drives," *IEEE Trans. Power Electron.*, vol. 30, no. 4, pp. 2363–2371, April 2015.

[42] C. Schauder, "Adaptive speed identification for vector control of induction motors without rotational transducers," *IEEE Trans. Ind. Appl.*, vol. 28, no. 5, pp. 1054–1061, 1992.

[43] K. Hurst, T. Habetler, G. Griva, and F. Profumo, "Zero-speed tacholess IM torque control: simply a matter of stator voltage integration," *IEEE Trans. Ind. Appl.*, vol. 34, no. 4, pp. 790–795, 1998.

[44] M.-H. Shin, D.-S. Hyun, S.-B. Cho, and S.-Y. Choe, "An improved stator flux estimation for speed sensorless stator flux orientation control of induction motors," *IEEE Trans. Power Electron.*, vol. 15, no. 2, pp. 312–318, Mar 2000.

[45] L. Harnefors, M. Jansson, R. Ottersten, and K. Pietilainen, "Unified sensorless vector control of synchronous and induction motors," *IEEE Trans. Ind. Electron.*, vol. 50, no. 1, pp. 153–160, 2003.

[46] N. R. N. Idris and A. H. M. Yatim, "An improved stator flux estimation in steady-state operation for direct torque control of induction machines," *IEEE Trans. Ind. Appl.*, vol. 38, no. 1, pp. 110–116, Jan 2002.

[47] M. Hinkkanen and J. Luomi, "Modified integrator for voltage model flux estimation of induction motors," *IEEE Trans. Ind. Electron.*, vol. 50, no. 4, pp. 818–820, aug 2003.

[48] M. Comanescu and L. Xu, "An improved flux observer based on PLL frequency estimator for sensorless vector control of induction motors," *IEEE Trans. Ind. Electron.*, vol. 53, no. 1, pp. 50–56, feb 2006.

[49] G.-R. Chen, J.-Y. Chen, and S.-C. Yang, "Implementation issues of flux linkage estimation on permanent magnet machine position sensorless drive at low speed," *IEEE Access*, vol. 7, pp. 164 641–164 649, 2019.

[50] M. Jansson, L. Harnefors, O. Wallmark, and M. Leksell, "Synchronization at startup and stable rotation reversal of sensorless nonsalient pmsm drives," *IEEE Trans. Ind. Electron.*, vol. 53, no. 2, pp. 379–387, 2006.

[51] M. Rahman, M. Haque, L. Tang, and L. Zhong, "Problems associated with the direct torque control of an interior permanent-magnet synchronous motor drive and their remedies," *IEEE Trans. Ind. Electron.*, vol. 51, no. 4, pp. 799–809, aug 2004.

[52] B. Li and L. Li, "New integration algorithms for flux estimation of AC machines," in *2011 International Conference on Electrical Machines and Systems*. IEEE, aug 2011.

[53] J. Hu and B. Wu, "New integration algorithms for estimating motor flux over a wide speed range," *IEEE Trans. Power Electron.*, vol. 13, no. 5, pp. 969–977, Sep 1998.

[54] N. Matsui, "Sensorless pm brushless dc motor drives," *IEEE Trans. Ind. Electron.*, vol. 43, no. 2, pp. 300–308, April 1996.

[55] M. Preindl and E. Schaltz, "Sensorless model predictive direct current control using novel second-order PLL observer for PMSM drive systems," *IEEE Trans. Ind. Electron.*, vol. 58, no. 9, pp. 4087–4095, sep 2011.

[56] J.-K. Seok, J.-K. Lee, and D.-C. Lee, "Sensorless speed control of non-salient permanent-magnet synchronous motor using rotor-position-tracking pi controller," *IEEE Trans. Ind. Electron.*, vol. 53, no. 2, pp. 399–405, 2006.

[57] H. Tajima, Y. Matsumoto, and H. Umida, "Speed sensorless vector control method for an industrial drive system," *IEEJ Transactions on Industry Applications*, vol. 116, no. 11, pp. 1103–1109, 1996.

[58] K. H. Nam, *AC Motor Control and Electrical Vehicle Applications (1st ed.)*. CRC Press, 2010.

[59] T. Tuovinen, M. Hinkkanen, L. Harnefors, and J. Luomi, "Comparison of a reduced-order observer and a full-order observer for sensorless synchronous motor drives," *IEEE Trans. Ind. Appl.*, vol. 48, no. 6, pp. 1959–1967, 2012.

[60] L. A. Jones and J. H. Lang, "A state observer for the permanent-magnet synchronous motor," *IEEE Trans. Ind. Electron.*, vol. 36, no. 3, pp. 374–382, 1989.

[61] C. Lascu and G.-D. Andreescu, "PLL position and speed observer with integrated current observer for sensorless PMSM drives," *IEEE Trans. Ind. Electron.*, vol. 67, no. 7, pp. 5990–5999, jul 2020.

[62] M. Hinkkanen, S. E. Saarakkala, H. A. A. Awan, E. Mölsä, and T. Tuovinen, "Observers for sensorless synchronous motor drives: Framework for design and analysis," *IEEE Trans. Ind. Appl.*, vol. 54, no. 6, pp. 6090–6100, 2018.

[63] J. Maes and J. A. Melkebeek, "Speed-sensorless direct torque control of induction motors using an adaptive flux observer," *IEEE Trans. Ind. Appl.*, vol. 36, no. 3, pp. 778–785, May 2000.

[64] M. Kim and S.-K. Sul, "An enhanced sensorless control method for PMSM in rapid accelerating operation," in *The 2010 International Power Electronics Conference - ECCE ASIA -*. IEEE, jun 2010.

[65] S. Ye and X. Yao, "A modified flux sliding-mode observer for the sensorless control of PMSMs with online stator resistance and inductance estimation," *IEEE Trans. Power Electron.*, vol. 35, no. 8, pp. 8652–8662, aug 2020.

[66] S. Shinnaka, "New "d-state-observer"-based vector control for sensorless drive of permanent-magnet synchronous motors," *IEEE Trans. Ind. Appl.*, vol. 41, no. 3, pp. 825–833, may 2005.

[67] S. Doki, S. Sangwongwanich, and S. Okuma, "Implementation of speed-sensor-less field-oriented vector control using adaptive sliding observers," in *Proceedings of the 1992 International Conference on Industrial Electronics, Control, Instrumentation, and Automation*, Nov 1992, pp. 453–458 vol.1.

[68] C. J. Volpato Filho and R. P. Vieira, "Adaptive full-order observer analysis and design for sensorless interior permanent magnet synchronous motors drives," *IEEE Trans. Ind. Electron.*, vol. 68, no. 8, pp. 6527–6536, 2021.

[69] D. Xiao, S. Nalakath, Y. Sun, J. Wiseman, and A. Emadi, "Complex-coefficient adaptive disturbance observer for position estimation of IPMSMs with robustness to DC errors," *IEEE Trans. Ind. Electron.*, vol. 67, no. 7, pp. 5924–5935, jul 2020.

[70] S. Bolognani, S. Calligaro, and R. Petrella, "Design issues and estimation errors analysis of back-EMF based position and speed observer for SPM synchronous motors," in *2011 Symposium on Sensorless Control for Electrical Drives*. IEEE, sep 2011.

[71] Z. Xu and M. Rahman, "An adaptive sliding stator flux observer for a direct-torque-controlled IPM synchronous motor drive," *IEEE Trans. Ind. Electron.*, vol. 54, no. 5, pp. 2398–2406, oct 2007.

[72] S. Sayeef, G. Foo, and M. F. Rahman, "Rotor position and speed estimation of a variable structure direct-torque-controlled IPM synchronous motor drive at very low speeds including standstill," *IEEE Trans. Ind. Electron.*, vol. 57, no. 11, pp. 3715–3723, nov 2010.

[73] Z. Xu and M. F. Rahman, "Comparison of a sliding observer and a kalman filter for direct-torque-controlled IPM synchronous motor drives," *IEEE Trans. Ind. Electron.*, vol. 59, no. 11, pp. 4179–4188, nov 2012.

[74] G. Wang, Z. Li, G. Zhang, Y. Yu, and D. Xu, "Quadrature PLL-based high-order sliding-mode observer for IPMSM sensorless control with online MTPA control strategy," *IEEE Trans. Energy Convers.*, vol. 28, no. 1, pp. 214–224, mar 2013.

[75] M. Tomita, T. Senjyu, S. Doki, and S. Okuma, "New sensorless control for brushless dc motors using disturbance observers and adaptive velocity estimations," *IEEE Trans. Ind. Electron.*, vol. 45, no. 2, pp. 274–282, Apr 1998.

[76] Z. Chen, M. Tomita, S. Doki, and S. Okuma, "An extended electromotive force model for sensorless control of interior permanent-magnet synchronous motors," *IEEE Trans. Ind. Electron.*, vol. 50, no. 2, pp. 288–295, Apr 2003.

[77] C. J. Volpato Filho and R. P. Vieira, "Pole placement design methodology of back-emf adaptive observer for sensorless pmsm drives," *Journal of Control, Automation and Electrical Systems*, vol. 31, no. 1, pp. 84–93, 2020.

[78] F. Jiang, S. Sun, A. Liu, Y. Xu, Z. Li, X. Liu, and K. Yang, "Robustness improvement of model-based sensorless SPMSM drivers based on an adaptive extended state observer and an enhanced quadrature PLL," *IEEE Trans. Power Electron.*, vol. 36, no. 4, pp. 4802–4814, apr 2021.

[79] W. Zhao, S. Jiao, Q. Chen, D. Xu, and J. Ji, "Sensorless control of a linear permanent-magnet motor based on an improved disturbance observer," *IEEE Trans. Ind. Electron.*, vol. 65, no. 12, pp. 9291–9300, dec 2018.

[80] H. Kim, M. C. Harke, and R. D. Lorenz, "Sensorless control of interior permanent-magnet machine drives with zero-phase lag position estimation," *IEEE Trans. Ind. Appl.*, vol. 39, no. 6, pp. 1726–1733, 2003.

[81] B. Du, S. Wu, S. Han, and S. Cui, "Application of linear active disturbance rejection controller for sensorless control of internal permanent-magnet synchronous motor," *IEEE Trans. Ind. Electron.*, vol. 63, no. 5, pp. 3019–3027, may 2016.

[82] L. Qu, W. Qiao, and L. Qu, "An enhanced linear active disturbance rejection rotor position sensorless control for permanent magnet synchronous motors," *IEEE Trans. Power Electron.*, vol. 35, no. 6, pp. 6175–6184, jun 2020.

[83] S. Morimoto, K. Kawamoto, M. Sanada, and Y. Takeda, "Sensorless control strategy for salient-pole pmsm based on extended emf in rotating reference frame," *IEEE Trans. Ind. Appl.*, vol. 38, no. 4, pp. 1054–1061, 2002.

[84] S. Chi, Z. Zhang, and L. Xu, "Sliding-mode sensorless control of direct-drive pm synchronous motors for washing machine applications," *IEEE Trans. Ind. Appl.*, vol. 45, no. 2, pp. 582–590, 2009.

[85] H. Kim, J. Son, and J. Lee, "A high-speed sliding-mode observer for the sensorless speed control of a pmsm," *IEEE Trans. Ind. Electron.*, vol. 58, no. 9, pp. 4069–4077, Sept 2011.

[86] Z. Qiao, T. Shi, Y. Wang, Y. Yan, C. Xia, and X. He, "New sliding-mode observer for position sensorless control of permanent-magnet synchronous motor," *IEEE Trans. Ind. Electron.*, vol. 60, no. 2, pp. 710–719, Feb 2013.

[87] L. Zhang, Y. Fan, C. Li, A. Nied, and M. Cheng, "Fault-tolerant sensorless control of a five-phase FTFSCW-IPM motor based on a wide-speed strong-robustness sliding mode observer," *IEEE Trans. Energy Convers.*, vol. 33, no. 1, pp. 87–95, mar 2018.

[88] K.-L. Kang, J.-M. Kim, K.-B. Hwang, and K.-H. Kim, "Sensorless control of pmsm in high speed range with iterative sliding mode observer," in *Nineteenth Annual IEEE Applied Power Electronics Conference and Exposition, 2004. APEC'04.*, vol. 2. IEEE, 2004, pp. 1111–1116.

[89] Y. Feng, J. Zheng, X. Yu, and N. V. Truong, "Hybrid terminal sliding-mode observer design method for a permanent-magnet synchronous motor control system," *IEEE Trans. Ind. Electron.*, vol. 56, no. 9, pp. 3424–3431, 2009.

[90] A. Apte, V. A. Joshi, H. Mehta, and R. Walambe, "Disturbance-observer-based sensorless control of PMSM using integral state feedback controller," *IEEE Trans. Power Electron.*, vol. 35, no. 6, pp. 6082–6090, jun 2020.

[91] D. Zaltni, M. Ghanes, J. P. Barbot, and M. N. Abdelkrim, "A HOSM observer with an improved zero-speed position estimation design for surface PMSM sensor-less control," in *2010 IEEE International Conference on Control Applications*. IEEE, sep 2010.

[92] L. Zhao, J. Huang, H. Liu, B. Li, and W. Kong, "Second-order sliding-mode observer with online parameter identification for sensorless induction motor drives," *IEEE Trans. Ind. Electron.*, vol. 61, no. 10, pp. 5280–5289, 2014.

[93] D. Liang, J. Li, R. Qu, and W. Kong, "Adaptive second-order sliding-mode observer for pmsm sensorless control considering vsi nonlinearity," *IEEE Trans. Power Electron.*, vol. 33, no. 10, pp. 8994–9004, Oct 2018.

[94] M. Morawiec and A. Lewicki, "Speed observer structure of induction machine based on sliding super-twisting and backstepping techniques," *IEEE Trans. Ind. Informat.*, vol. 17, no. 2, pp. 1122–1131, feb 2021.

[95] A. T. Woldegiorgis, X. Ge, S. Li, and M. Hassan, "Extended sliding mode disturbance observer-based sensorless control of IPMSM for medium and high-speed range considering railway application," *IEEE Access*, vol. 7, pp. 175 302–175 312, 2019.

[96] S. Chung, "Robust speed control of brushless direct-drive motor using integral variable structure control," *IEE Proceedings - Electric Power Applications*, vol. 142, no. 6, p. 361, 1995.

[97] I. Sami, S. Ullah, A. Basit, N. Ullah, and J.-S. Ro, "Integral super twisting sliding mode based sensorless predictive torque control of induction motor," *IEEE Access*, vol. 8, pp. 186 740–186 755, 2020.

[98] W. Xu, S. Qu, L. Zhao, and H. Zhang, "An improved adaptive sliding mode observer for middle- and high-speed rotor tracking," *IEEE Trans. Power Electron.*, vol. 36, no. 1, pp. 1043–1053, jan 2021.

[99] J.-J. E. Slotine and W. Li, *Applied nonlinear control*. Prentice hall Englewood Cliffs, NJ, 1991, vol. 199, no. 1.

[100] M. Zhou, S. Cheng, Y. Feng, W. Xu, L. Wang, and W. Cai, "Full-order terminal sliding-mode-based sensorless control of induction motor with gain adaptation," *IEEE Trans. Emerg. Sel. Topics Power Electron.*, vol. 10, no. 2, pp. 1978–1991, 2022.

[101] H. Lee and J. Lee, "Design of iterative sliding mode observer for sensorless PMSM control," *IEEE Trans. Control Syst. Technol.*, vol. 21, no. 4, pp. 1394–1399, jul 2013.

[102] G. Foo and M. Rahman, "Sensorless sliding-mode MTPA control of an IPM synchronous motor drive using a sliding-mode observer and HF signal injection," *IEEE Trans. Ind. Electron.*, vol. 57, no. 4, pp. 1270–1278, apr 2010.

[103] Y. Wang, Y. Xu, and J. Zou, "Sliding-mode sensorless control of pmsm with inverter nonlinearity compensation," *IEEE Trans. Power Electron.*, vol. 34, no. 10, pp. 10 206–10 220, Oct 2019.

[104] G. Wang, R. Yang, and D. Xu, "DSP-based control of sensorless IPMSM drives for wide-speed-range operation," *IEEE Trans. Ind. Electron.*, vol. 60, no. 2, pp. 720–727, feb 2013.

[105] C. Lascu, I. Boldea, and F. Blaabjerg, "Comparative study of adaptive and inherently sensorless observers for variable-speed induction-motor drives," *IEEE Trans. Ind. Electron.*, vol. 53, no. 1, pp. 57–65, feb 2006.

[106] J. Chen and J. Huang, "Alternative solution regarding problems of adaptive observer compensating parameters uncertainties for sensorless induction motor drives," *IEEE Trans. Ind. Electron.*, vol. 67, no. 7, pp. 5879–5888, July 2020.

[107] F.-J. Lin, R.-J. Wai, and P.-C. Lin, "Robust speed sensorless induction motor drive," *IEEE Trans. Aerosp. Electron. Syst.*, vol. 35, no. 2, pp. 566–578, apr 1999.

[108] H. Rehman, A. Derdiyok, M. Guven, and L. Xu, "A new current model flux observer for wide speed range sensorless control of an induction machine," *IEEE Trans. Power Electron.*, vol. 17, no. 6, pp. 1041–1048, nov 2002.

[109] A. Derdiyok, M. Guven, H. Rehman, N. Inanc, and L. Xu, "Design and implementation of a new sliding-mode observer for speed-sensorless control of induction machine," *IEEE Trans. Ind. Electron.*, vol. 49, no. 5, pp. 1177–1182, oct 2002.

[110] G. Edelbaher, K. Jezernik, and E. Urlep, "Low-speed sensorless control of induction machine," *IEEE Trans. Ind. Electron.*, vol. 53, no. 1, pp. 120–129, feb 2006.

[111] Z. Zhang, H. Xu, L. Xu, and L. Heilman, "Sensorless direct field-oriented control of three-phase induction motors based on "sliding mode" for washing-machine drive applications," *IEEE Trans. Ind. Appl.*, vol. 42, no. 3, pp. 694–701, may 2006.

[112] H. Sira-Ramírez, A. Luviano-Juárez, M. Ramírez-Neria, and E. W. Zurita-Bustamante, *Active disturbance rejection control of dynamic systems: a flatness based approach*. Butterworth-Heinemann, 2018.

[113] A. A. Godbole, J. P. Kolhe, and S. E. Talole, "Performance analysis of generalized extended state observer in tackling sinusoidal disturbances," *IEEE Trans. Control Syst. Technol.*, vol. 21, no. 6, pp. 2212–2223, nov 2013.

[114] Y. Zuo, J. Chen, X. Zhu, and C. H. T. Lee, "Different active disturbance rejection controllers based on the same order gpi observer," *IEEE Trans. Ind. Electron.*, pp. 1–1, 2021.

[115] T. Senjyu, T. Shingaki, and K. Uezato, "Sensorless vector control of synchronous reluctance motors with disturbance torque observer," in *APEC 2000. Fifteenth Annual IEEE Applied Power Electronics Conference and Exposition (Cat. No.00CH37058)*. IEEE, 2000.

[116] Y. Yoon, S. Sul, S. Morimoto, and K. Ide, "High-bandwidth sensorless algorithm for ac machines based on square-wave-type voltage injection," *IEEE Trans. Ind. Appl.*, vol. 47, no. 3, pp. 1361–1370, May 2011.

[117] R. Lorenz and K. Van Patten, "High-resolution velocity estimation for all-digital, ac servo drives," *IEEE Trans. Ind. Appl.*, vol. 27, no. 4, pp. 701–705, 1991.

[118] T. Zhang, Z. Xu, J. Li, H. Zhang, and C. Gerada, "A third-order super-twisting extended state observer for dynamic performance enhancement of sensorless IPMSM drives," *IEEE Trans. Ind. Electron.*, vol. 67, no. 7, pp. 5948–5958, jul 2020.

[119] T. Zhang, Z. Xu, and C. Gerada, "A nonlinear extended state observer for sensorless IPMSM drives with optimized gains," *IEEE Trans. Ind. Appl.*, vol. 56, no. 2, pp. 1485–1494, mar 2020.

[120] Z. Xu, T. Zhang, Y. Bao, H. Zhang, and C. Gerada, "A nonlinear extended state observer for rotor position and speed estimation for sensorless IPMSM drives," *IEEE Trans. Power Electron.*, vol. 35, no. 1, pp. 733–743, jan 2020.

[121] S. R. Bowes, A. Sevinc, and D. Holliday, "New natural observer applied to speed-sensorless dc servo and induction motors," *IEEE Trans. Ind. Electron.*, vol. 51, no. 5, pp. 1025–1032, Oct 2004.

[122] L. Harnefors and H.-P. Nee, "A general algorithm for speed and position estimation of ac motors," *IEEE Trans. Ind. Electron.*, vol. 47, no. 1, pp. 77–83, 2000.

[123] J. S. Lee, R. D. Lorenz, and M. A. Valenzuela, "Time-optimal and loss-minimizing deadbeat-direct torque and flux control for interior permanent-magnet synchronous machines," *IEEE Trans. Ind. Appl.*, vol. 50, no. 3, pp. 1880–1890, 2014.

[124] L. Harnefors, "Instability phenomena and remedies in sensorless indirect field oriented control," *IEEE Trans. Power Electron.*, vol. 15, no. 4, pp. 733–743, Jul 2000.

[125] G. Yang and T. H. Chin, "Adaptive-speed identification scheme for a vector-controlled speed sensorless inverter-induction motor drive," *IEEE Trans. Ind. Appl.*, vol. 29, no. 4, pp. 820–825, Jul 1993.

[126] G. Yang and T.-H. Chin, "Hyperstability of the full-order observer for vector-controlled induction motor drive without speed sensor," *Elect. Eng. Jpn.*, vol. 113, p. 109–118, 1993.

[127] K. Kubota and K. Matsuse, "Speed sensorless field-oriented control of induction motor with rotor resistance adaptation," *IEEE Trans. Ind. Appl.*, vol. 30, no. 5, pp. 1219–1224, Sep 1994.

[128] H. Kubota, I. Sato, Y. Tamura, K. Matsuse, H. Ohta, and Y. Hori, "Regenerating-mode low-speed operation of sensorless induction motor drive with adaptive observer," *IEEE Trans. Ind. Appl.*, vol. 38, no. 4, pp. 1081–1086, Jul 2002.

[129] H. Tajima, G. Guidi, and H. Umida, "Consideration about problems and solutions of speed estimation method and parameter tuning for speed-sensorless vector control of induction motor drives," *IEEE Trans. Ind. Appl.*, vol. 38, no. 5, pp. 1282–1289, 2002.

[130] M. S. Zaky, M. K. Metwaly, H. Z. Azazi, and S. A. Deraz, "A new adaptive smo for speed estimation of sensorless induction motor drives at zero and very low frequencies," *IEEE Trans. Ind. Electron.*, vol. 65, no. 9, pp. 6901–6911, 2018.

[131] C. Luo, B. Wang, Y. Yu, Y. Zhu, and D. Xu, "Enhanced low-frequency ride-through for speed-sensorless induction motor drives with adaptive observable margin," *IEEE Trans. Ind. Electron.*, vol. 68, no. 12, pp. 11 918–11 930, 2021.

[132] N.-D. Nguyen, N. N. Nam, C. Yoon, and Y. I. Lee, "Speed sensorless model predictive torque control of induction motors using a modified adaptive full-order observer," *IEEE Trans. Ind. Electron.*, vol. 69, no. 6, pp. 6162–6172, 2022.

[133] P. Vas, *Sensorless vector and direct torque control*. Oxford University Press, USA, 1998.

[134] X. Zhang, "Sensorless induction motor drive using indirect vector controller and sliding-mode observer for electric vehicles," *IEEE Trans. Veh. Technol.*, vol. 62, no. 7, pp. 3010–3018, sep 2013.

[135] S. Suwankawin and S. Sangwongwanich, "Design strategy of an adaptive full-order observer for speed-sensorless induction-motor drives-tracking performance and stabilization," *IEEE Trans. Ind. Electron.*, vol. 53, no. 1, pp. 96–119, Feb 2006.

[136] E. Etien, C. Chaigne, and N. Bensiali, "On the stability of full adaptive observer for induction motor in regenerating mode," *IEEE Trans. Ind. Electron.*, vol. 57, no. 5, pp. 1599–1608, May 2010.

[137] S. Sangwongwanich, S. Suwankawin, S. Po-ngam, and S. Koonlaboon, "A unified speed estimation design framework for sensorless ac motor drives based on positive-real property," in *2007 Power Conversion Conference - Nagoya*, April 2007, pp. 1111–1118.

[138] W. Sun, Y. Yu, G. Wang, B. Li, and D. Xu, "Design method of adaptive full order observer with or without estimated flux error in speed estimation algorithm," *IEEE Trans. Power Electron.*, vol. 31, no. 3, pp. 2609–2626, mar 2016.

[139] M. Hinkkanen and J. Luomi, "Stabilization of regenerating-mode operation in sensorless induction motor drives by full-order flux observer design," *IEEE Trans. Ind. Electron.*, vol. 51, no. 6, pp. 1318–1328, Dec 2004.

[140] J. Chen and J. Huang, "Stable simultaneous stator and rotor resistances identification for speed sensorless im drives: Review and new results," *IEEE Trans. Power Electron.*, vol. 33, no. 10, pp. 8695–8709, Oct 2018.

[141] L. Harnefors and M. Hinkkanen, "Stabilization methods for sensorless induction motor drives — a survey," *IEEE Trans. Emerg. Sel. Topics Power Electron.*, vol. 2, no. 2, pp. 132–142, June 2014.

[142] H. Tajima and Y. Hori, "Speed sensorless field-orientation control of the induction machine," *IEEE Trans. Ind. Appl.*, vol. 29, no. 1, pp. 175–180, 1993.

[143] M. Comanescu and L. Xu, "Sliding-mode MRAS speed estimators for sensorless vector control of induction machine," *IEEE Trans. Ind. Electron.*, vol. 53, no. 1, pp. 146–153, feb 2006.

[144] M. Amin, G. A. A. Aziz, and J. Durkin, "A robust simplified dynamic observer-based backstepping control of six-phase induction motor for marine vessels applications," in *2019 IEEE Industry Applications Society Annual Meeting*. IEEE, sep 2019.

[145] J. Chen and J. Huang, "Online decoupled stator and rotor resistances adaptation for speed sensorless induction motor drives by a time-division approach," *IEEE Trans. Power Electron.*, vol. 32, no. 6, pp. 4587–4599, June 2017.

[146] L. Harnefors, "Design and analysis of general rotor-flux-oriented vector control systems," *IEEE Trans. Ind. Electron.*, vol. 48, no. 2, pp. 383–390, April 2001.

[147] C. Lascu, I. Boldea, and F. Blaabjerg, "A class of speed-sensorless sliding-mode observers for high-performance induction motor drives," *IEEE Trans. Ind. Electron.*, vol. 56, no. 9, pp. 3394–3403, sep 2009.

[148] M. H. Holakooie, M. Ojaghi, and A. Taheri, "Modified DTC of a six-phase induction motor with a second-order sliding-mode MRAS-based speed estimator," *IEEE Trans. Power Electron.*, vol. 34, no. 1, pp. 600–611, jan 2019.

[149] M. Korzonek, G. Tarchala, and T. Orlowska-Kowalska, "A review on mras-type speed estimators for reliable and efficient induction motor drives," *ISA transactions*, 2019.

[150] P. Kudva and K. S. Narendra, "Synthesis of an adaptive observer using lyapunov's direct method," *International Journal of Control*, vol. 18, no. 6, pp. 1201–1210, 1973.

[151] R. Marino and P. Tomei, "Global adaptive observers for nonlinear systems via filtered transformations," *IEEE Trans. Autom. Control*, vol. 37, no. 8, pp. 1239–1245, Aug 1992.

[152] Q. Zhang, "Adaptive observer for multiple-input-multiple-output (mimo) linear time-varying systems," *IEEE Trans. Autom. Control*, vol. 47, no. 3, pp. 525–529, Mar 2002.

[153] L. Harnefors, "Globally stable speed-adaptive observers for sensorless induction motor drives," *IEEE Trans. Ind. Electron.*, vol. 54, no. 2, pp. 1243–1245, April 2007.

[154] M. Farza, M. M'Saad, T. Maatoug, and M. Kamoun, "Adaptive observers for nonlinearly parameterized class of nonlinear systems," *Automatica*, vol. 45, no. 10, pp. 2292–2299, 2009.

[155] M. Farza, M. M'Saad, T. Ménard, A. Ltaief, and T. Maatoug, "Adaptive observer design for a class of nonlinear systems. application to speed sensorless induction motor," *Automatica*, vol. 90, pp. 239–247, 2018.

[156] R. Marino, P. Tomei, and C. M. Verrelli, *Induction motor control design*. Springer London, 2010.

[157] Y. Zheng and K. A. Loparo, "Adaptive flux and speed estimation for induction motors," in *Proceedings of the 1999 American Control Conference (Cat. No. 99CH36251)*, vol. 4, 1999, pp. 2521–2525 vol.4.

[158] J. Chen and J. Huang, "Globally stable speed-adaptive observer with auxiliary states for sensorless induction motor drives," *IEEE Trans. Power Electron.*, vol. 34, no. 1, pp. 33–39, Jan 2019.

[159] J. Chen, J. Huang, and Y. Sun, "Resistances and speed estimation in sensorless induction motor drives using a model with known regressors," *IEEE Trans. Ind. Electron.*, vol. 66, no. 4, pp. 2659–2667, April 2019.

[160] J. Chen and J. Huang, "Application of adaptive observer to sensorless induction motor via parameter-dependent transformation," *IEEE Trans. Control Syst. Technol.*, vol. 27, no. 6, pp. 2630–2637, Nov 2019.

[161] A. Dib, M. Farza, M. M'Saad, P. Dorleans, and J.-F. Massieu, "High gain observer for sensorless induction motor," *IFAC Proceedings Volumes*, vol. 44, no. 1, pp. 674–679, 2011.

[162] C. Du, Z. Yin, J. Liu, Y. Zhang, and X. Sun, "A speed estimation method for induction motors based on active disturbance rejection observer," *IEEE Trans. Power Electron.*, vol. 35, no. 8, pp. 8429–8442, aug 2020.

[163] M. Koteich, A. Maloum, G. Duc, and G. Sandou, "Local weak observability conditions of sensorless ac drives," in *2015 17th European Conference on Power Electronics and Applications (EPE'15 ECCE-Europe)*, 2015, pp. 1–10.

[164] ——, "Permanent magnet synchronous drives observability analysis for motion-sensorless control," in *2015 IEEE Symposium on Sensorless Control for Electrical Drives (SLED)*, 2015, pp. 1–8.

[165] L. Harnefors and M. Hinkkanen, "Complete stability of reduced-order and full-order observers for sensorless im drives," *IEEE Trans. Ind. Electron.*, vol. 55, no. 3, pp. 1319–1329, March 2008.

[166] F. Garofalo and L. Glielmo, *Robust control via variable structure and Lyapunov techniques*. Springer, 1996, vol. 217.